Published in final edited form as:

Nature. 2019 April ; 568(7752): 351–356. doi:10.1038/s41586-019-1100-z.

Nitrosative Stress Drives Heart Failure with Preserved Ejection Fraction

Gabriele G. Schiattarella[1,2], **Francisco Altamirano**[1], **Dan Tong**[1], **Kristin M. French**[1], **Elisa Villalobos**[1], **Soo Young Kim**[1], **Xiang Luo**[1], **Nan Jiang**[1], **Herman I. May**[1], **Zhao V. Wang**[1], **Theodore M. Hill**[1], **Pradeep P.A. Mammen**[1], **Jian Huang**[1], **Dong Ik Lee**[3], **Virginia Hahn**[3], **Kavita Sharma**[3], **David A. Kass**[3], **Sergio Lavandero**[1,4], **Thomas G. Gillette**[1], and **Joseph A. Hill**[1,5]

[1]Department of Internal Medicine (Cardiology), University of Texas Southwestern Medical Center, Dallas, Texas, USA, 75390-8573 [2]Department of Advanced Biomedical Sciences, Federico II University, 80131 Naples, Italy [3]Department of Medicine (Cardiology), Johns Hopkins School of Medicine, Baltimore, Maryland [4]Advanced Center for Chronic Diseases (ACCDiS) & Center for Molecular Studies of the Cell (CEMC), Faculty of Chemical & Pharmaceutical Sciences & Faculty of Medicine, University of Chile, Santiago 8380492, Chile [5]Department of Molecular Biology, University of Texas Southwestern Medical Center, Dallas, Texas, USA, 75390-8573

Abstract

Heart failure with preserved ejection fraction (HFpEF) is a common, morbid, and mortal syndrome for which there are no evidence-based therapies. Here, we report that concomitant metabolic and hypertensive stress in mice elicited by a combination of high fat diet (HFD) and constitutive nitric oxide (NO) synthase inhibition by N[ω]-nitro-l-arginine methyl ester (L-NAME) recapitulates the numerous systemic and cardiovascular features of human HFpEF. One of the unfolded protein response (UPR) effectors, the spliced form of X-box binding protein 1 (Xbp1s), was reduced in the myocardium of both experimental and human HFpEF. Mechanistically, the

Author Information. Reprints and permissions information is available at www.nature.com/reprints.

Correspondence and requests for materials should be addressed: Joseph A. Hill, M.D., Ph.D., Division of Cardiology, University of Texas Southwestern Medical Center, 6000 Harry Hines Blvd, NB11.200, Dallas, Texas, 75390-8573, Tel: 1-214-648-1400, Fax: 1-214-648-1450, joseph.hill@utsouthwestern.edu.

Author Contributions. G.G.S., F.A., D.T., K.F., E.V. S.Y.K performed the experiments. G.G.S. designed the experiments, performed the analyses and wrote the manuscript. F.A. designed the nitrosylation experiments, performed the analysis, isolated the AMVMs and performed the contractility studies. X.L. isolated the NRVMs. N.J. managed mouse colonies. H.I.M. performed the PV loop experiments and mouse surgeries. Z.V.W. provided the Xbp1sTG mice and Xbp1s adenovirus. P.P.A.M., J.H performed the skeletal muscle experiments, D.I.L., V.H., D.A.K. provided human data. S.L., T.G.G. contributed to the experimental design and manuscript preparation, J.A.H. conceived the project and contributed to manuscript preparation.

Supplementary Information is available in the online version of the paper.

Competing Interests Declaration. G.G.S., T.G.G., and J.A.H. are co-inventors on a patent application (PCT/US/2017/037019) that was filed in June 2017 (provisional filed in June 2016). The patent relates to the diet used for modeling HFpEF.

Data availability

The authors declare that the data supporting the findings of this study are available within the paper and its Supplementary Information. Each data point corresponding to figures that describe the results from in vivo/in vitro model studies are provided as separate Source Data for Figs. 1c, d, f–i, 2a, d, f, g, i–m, 3a–d, f, g, I, j, 4a–d, f, h, Extended Data Fig. 1a–l, Extended Data Fig. 2b–f, Extended Data Fig. 3b–d, e, g, Extended Data Fig. 4a–l, n, p, Extended Data Fig. 5b–g, Extended Data Fig. 6b–g, j–m, Extended Data Fig. 7b, d, g, Extended Data Fig. 8b–d, g, Extended Data Fig. 9c–i and Extended Data Fig. 10b–i. Other source data related to the study are available from the corresponding author upon reasonable request

decrease in Xbp1s resulted from increased inducible NO synthase (iNOS) activity and S-nitrosylation of endonuclease inositol-requiring protein 1α (IRE1α), culminating in defective Xbp1 splicing. Pharmacological or genetic suppression of iNOS, or cardiomyocyte-restricted overexpression of Xbp1s, each ameliorated the HFpEF phenotype. We have unveiled iNOS-driven dysregulation of IRE1α-Xbp1s as a crucial mechanism of cardiomyocyte dysfunction in HFpEF.

HFpEF is a burgeoning public health problem, accounting for approximately half of HF hospital admissions[1]. The complex clinical phenotype that characterizes this syndrome stems from the presence of multiple comorbidities, including obesity, hypertension and diabetes[2]. Clinical data suggest that systemic inflammation and imbalance in NO levels are crucial for development of HFpEF[3]. However, definitive experimental evidence supporting these concepts has not emerged owing to limitations in preclinical models that fail to recapitulate the full range of the syndrome's features. As a result, fundamental pathophysiological mechanisms remain obscure, and there are no evidence-based clinical therapies available for these individuals[2,4,5].

A novel "two-hit" mouse model of HFpEF

As patients with HFpEF very often harbor the comorbidities of hypertension and obesity/metabolic dysfunction[2], we formulated a "two-hit" hypothesis, one in which the coincidence of metabolic stress (obesity/metabolic syndrome) and mechanical stress (hypertension) induced by NO dysregulation is a major mechanism underlying HFpEF pathophysiology. To test this, male C57BL/6N wild-type mice were divided into four treatment groups and exposed to 1) HFD (60% calories from lard); 2) L-NAME (0.5 g/L in drinking water); 3) a combination of both treatments (HFD+L-NAME); or 4) standard (CHOW) diet for five or fifteen weeks (Fig. 1a). As expected HFD feeding elicited body weight increases and glucose intolerance (Extended Data Fig. 1a–c), whereas L-NAME treatment raised both systolic and diastolic blood pressure (Extended Data Fig. 1d, e). Longitudinal echocardiographic evaluation revealed persistently preserved left ventricular ejection fraction (LVEF) in all groups (up to one year in the HFD+L-NAME cohort) (Fig. 1b, c, Extended Data Fig. 1f and Extended Data Table 1) coupled with significant alterations in LV global longitudinal strain uniquely in HFD+L-NAME mice at both 5- and 15-week time points (Fig. 1d and Extended Data Fig. 1g). Whereas varying degrees of diastolic dysfunction were observed in the different experimental groups, animals exposed to two "hits" (HFD+L-NAME) manifested signs of increased LV filling pressure as measured both by noninvasive Doppler (Fig. 1e, f, Extended Data Fig. 1h, i and Extended Data Table 1) and invasive (Extended Data Table 1) analyses. In accordance with the documented elevated filling pressures, mice exposed to HFD+L-NAME uniquely exhibited a robust increase in lung weight (Fig. 1g and Extended Data Fig. 1j), indicative of pulmonary congestion and a preclinical surrogate for HF. Cardiac (Fig. 1h and Extended Data Fig. 1k) and cardiomyocyte hypertrophy (Extended Data Fig. 2a, b), as well as cardiac fibrosis (Extended Data Fig. 2a, c) and myocardial capillary rarefaction (Extended Data Fig. 2a, d), were observed in mice treated with L-NAME or the combination of HFD+L-NAME. Chronic L-NAME administration also increased aortic stiffness measured by pulse wave velocity (Extended Data Fig. 2e) and impaired coronary artery endothelial function, reducing

coronary flow reserve (Extended Data Fig. 2f, g). Whereas excess weight impacted exercise performance (Fig. 1i and Extended Data Fig. 1l), after fifteen weeks of combination treatment, HFD+L-NAME mice displayed a significant reduction in running distance compared to the other cohorts (Fig. 1i). Importantly, exercise intolerance in HFD+L-NAME mice occurred in the absence of major histopathological (Extended Data Fig. 3a), molecular (Extended Data Fig. 3b), or strength (Extended Data Fig. 3c–f) abnormalities in skeletal muscle, suggesting that, during the period of observation here, the decrement in exercise tolerance in our HFpEF model is not due to a deficit in skeletal muscle function. Whereas some overlapping features were observed in L-NAME- and HFD-treated groups, the presence of the greatest hypertrophic response and worsened diastolic function, coupled with pulmonary congestion observed exclusively in the HFD+L-NAME group, lend additional support to the notion that this is a *bona fide* model of HFpEF. As abnormalities in cardiomyocyte contraction and relaxation are common features in HFpEF[6,7], adult ventricular myocytes were harvested after five weeks of dietary manipulation, revealing significant reductions in contraction velocity and impaired relaxation uniquely in the HFD +L-NAME cohort (Extended Data Fig. 4a–f).

Inactivation of IRE1α-Xbp1s signaling pathway in experimental and human HFpEF

Evidence thus far suggested that concomitant exposure to HFD+L-NAME elicits unique functional and structural changes in the heart that mirror the clinical features of human HFpEF. Seizing upon the recent observation that accumulation of misfolded proteins occurs in clinical HFpEF[8], we evaluated the unfolded protein response (UPR), an evolutionarily conserved adaptive response capable of mitigating stress in conditions that disrupt protein quality control[9]. The IRE1α-Xbp1 axis is the evolutionarily most conserved branch of the UPR, one that we recently identified as a novel regulator of cardiomyocyte stress responsiveness[10]. The role of the IRE1α-Xbp1 signaling pathway in HFpEF is unknown.

Analysis of transcript levels of multiple UPR markers in hearts from all four treatment groups at five weeks revealed activation of UPR sensors and effectors in HFD and L-NAME ("single-hit") mice (Fig. 2a). In HFD+L-NAME hearts, we detected no changes in activating transcription factor 6 (ATF6) transcript (Fig. 2a) and protein (Fig. 2b) levels and a mild activation of the protein kinase RNA-like ER kinase (PERK) branch (Fig. 2b). Surprisingly, however, we detected a significant reduction below baseline in the transcript levels of binding immunoglobulin protein (BIP), CCAAT-enhancer-binding protein homologous protein (CHOP) and Xbp1s uniquely in hearts (Fig. 2a, c) and cardiomyocytes (Fig. 2d) from HFD+L-NAME mice. Reduced levels of Xbp1s in HFD+L-NAME hearts was associated with a reduction in IRE1α phosphorylation (Fig. 2e, f). These observations were replicated in LV samples from a previously validated, rat model of HFpEF: the ZSF1-obese rats (Extended Data Fig. 4g–o).

In contrast with our findings in HFpEF rodents, we detected robust activation of this UPR pathway and increased Xbp1 splicing in a preclinical model of pressure overload-induced HF with reduced ejection fraction (HFrEF) induced by severe transverse aortic constriction

(sTAC)[11] (Extended Data Fig. 5a–i). In addition, in a model of milder pressure overload (TAC) prior to emergence of systolic dysfunction (three weeks), we observed similar levels of diastolic dysfunction and pulmonary congestion as in HFD+L-NAME mice (Extended Data Fig. 6a–f) but without reduction in myocardial Xbp1s transcript (Extended Data Fig. 6g) or reduction in IRE1α phosphorylation (Extended Data Fig. 6h), supporting the notion that in a TAC model the "HFpEF phenotype" is time delimited, in contrast with observations in HFD+L-NAME mice (Extended Data Table 1) and in patients[1].

To test for human relevance, we turned to endomyocardial biopsies of control and failing human hearts (Extended Data Table 2). Strikingly, and in accordance with our observations in both ZSF1-obese rats and HFD+L-NAME mice, Xbp1s transcript was also reduced uniquely in human HFpEF hearts, whereas the unspliced form of Xbp1 (Xbp1u) did not change among control, HFpEF, or HFrEF hearts (Fig. 2g). Accordingly, IRE1α phosphorylation levels were also down-regulated exclusively in human HFpEF myocardium (Fig. 2h, i). Together, these data confirm that defective IRE1α splicing activity and Xbp1s downregulation occur in both experimental and clinical HFpEF but not in HFrEF, suggesting distinct roles of this transcription factor in the two different types of HF.

As our findings reveal that down-regulation of Xbp1s correlated with the development of HFpEF, we utilized a cardiomyocyte-specific, doxycycline responsive Tet-off Xbp1s transgenic mouse line (TG)[10] to test for a causal role of Xbp1s in HFpEF pathogenesis. Five weeks of exposure of Xbp1s TG and littermate control (CTR) animals to the HFD+L-NAME regimen (Extended Data Fig. 6i) was sufficient to induce a cardiac phenotype characterized by diastolic dysfunction with preserved LVEF (Fig. 2j, k, and Extended Data Fig. 6j). Remarkably, two weeks of Xbp1s overexpression (Extended Data Fig. 6k) ameliorated diastolic dysfunction (Fig. 2j, k), improved exercise tolerance (Fig. 2l), reduced lung congestion (Fig. 2m) and decreased the expression of HF-related genes (Extended Data Fig. 6l) without impacting LVEF (Extended Data Fig. 6j) or cardiac hypertrophy (Extended Data Fig. 6m). Taken together, these data demonstrate that overexpression of Xbp1s in cardiomyocytes is sufficient to partially ameliorate the diastolic dysfunction and signs of HF observed in HFpEF mice, suggesting a model in which reduced abundance of Xbp1s in cardiomyocytes is a driving force in HFpEF pathogenesis.

Meta-inflammation-induced nitrosative stress elicits S-nitrosylation of IRE1α in HFpEF

As noted previously, the current paradigm of HFpEF pathophysiology holds that comorbidities drive cardiac remodeling in HFpEF through microvascular endothelial inflammation[12]. A systemic pro-inflammatory state reduces endothelial NOS (eNOS) activity in coronary endothelial cells limiting NO bioavailability for cardiomyocytes. In fact, in our model, L-NAME, which we use as a driver of endothelial dysfunction-based hypertension, is a substantially more potent inhibitor of eNOS and neuronal NOS (nNOS) as compared to inducible NOS (iNOS)[13,]. Interestingly, L-NAME-induced events are associated with up-regulation of iNOS in the cardiovascular system[14]. Similarly, iNOS is upregulated in rodents exposed to HFD[15]. These observations suggest that the

comorbidities-induced inflammatory state – metabolic inflammation (meta-inflammation) – observed in clinical HFpEF might be replicated by the combination of HFD+L-NAME, pointing to iNOS as a common disease feature.

The combination of HFD+L-NAME elicited a systemic pro-inflammatory state (Extended Data Fig. 7a, b) coupled with increased iNOS transcript (Fig. 3a) and protein (Extended Data Fig. 7c) levels in the myocardium relative to either treatment in isolation and in the absence of changes in eNOS transcript (Extended Data Fig. 7d) or eNOS and nNOS proteins (Extended Data Fig. 7e). Changes in iNOS levels were mirrored at the cardiomyocyte level (Fig. 3b). iNOS transcript was increased in LV samples from ZSF1-obese rats (Fig. 3c) as well, and importantly, uniquely in human HFpEF hearts (Fig. 3d) confirming increased abundance of iNOS in myocardium of both experimental and clinical HFpEF. Elevated iNOS activity and nitrosative stress promote S-nitrosylation of cysteine residues within multiple proteins and can perturb their function[16]. Accordingly, we observed a mild increase in total protein nitrosylation in hearts of HFD+L-NAME mice (Extended Data Fig. 7f, g).

The novel observations of increased iNOS coupled with reduced Xbp1s levels in the myocardium of both experimental and human HFpEF raised the possibility of a connection between iNOS activity and Xbp1s production. Liver from morbidly obese mice is marked by iNOS-dependent S-nitrosylation of IRE1α that inhibits its endonuclease activity, resulting in reduced Xbp1 splicing[15]. Strikingly, in HFD+L-NAME hearts, we observed aberrant S-nitrosylation of IRE1α (Fig. 3e, f). To determine whether this mechanism occurs in cardiomyocytes, neonatal rat ventricular myocytes (NRVMs) were infected with adenovirus driving iNOS expression (AdiNOS) (Extended Data Fig. 8a, b). Transduction of NRVMs with AdiNOS significantly increased NO production in NRVM culture medium (Extended Data Fig. 8c) without impacting cardiomyocyte viability (Extended Data Fig. 8d) and, importantly, resulted in a bi-phasic response in Xbp1s mRNA levels, with an initial rise and subsequent fall below basal levels (Fig. 3g). iNOS over-expression in cardiomyocytes was also sufficient to drive increases in global protein nitrosylation (Extended Data Fig. 8e) and IRE1α S-nitrosylation (Fig. 3h, i) in association with reduction in Xbp1s transcript levels (Fig. 3j). iNOS-dependent inhibition of IRE1α splicing activity was further corroborated by the observation of reduced IRE1α phosphorylation (Extended Data Fig. 8f) and blunted Xbp1s upregulation (Extended Data Fig. 8g) in ER-stressed cardiomyocytes.

To test directly for an effect of nitrosylation on IRE1α endoribonuclease activity, we employed an adenovirus encoding IRE1α harboring mutations in two target nitrosylation sites within the RNase domain[15]. Importantly, this mutant manifested significantly reduced iNOS-dependent IRE1α S-nitrosylation (Fig. 3h, i) coupled with a lack of nitrosylation-dependent suppression of Xbp1 splicing (Fig. 3j). Collectively, these results establish that iNOS governs IRE1α activity by increasing S-nitrosylation of IRE1α leading to reduction in Xbp1s generation in cardiomyocytes.

iNOS inhibition restores IRE1α-Xbp1s axis and ameliorates the HFpEF phenotype in mice

To confirm the critical role of iNOS-dependent suppression of the IRE1α-Xbp1s axis as contributing to HFpEF pathophysiology, iNOS knockout mice (iNOS KO; Extended Data Fig. 9a) were challenged with our HFpEF protocol (Extended Data Fig. 9b). Despite absence of differences in LVEF% (Extended Data Fig. 9c), body weight (Extended Data Fig. 9d), blood pressure (Extended Data Fig. 9e, f), glucose tolerance (Extended Data Fig. 9g, h), and cardiac hypertrophy (Extended Data Fig. 9i), significant attenuation of diastolic dysfunction (Fig. 4a, b), improvement in exercise tolerance (Fig. 4c), and reduced lung congestion (Fig. 4d) were observed in iNOS KO mice subjected to the HFD+L-NAME regimen. Importantly, under HFpEF conditions, iNOS gene ablation restored Xbp1 splicing (Fig. 4e) and Xbp1s transcript levels (Fig. 4f), as well as IRE1α phosphorylation (Fig. 4g, h). Notably, depletion of iNOS diminished global myocardial protein nitrosylation (Extended Data Fig. 7f, g), significantly reducing S-nitrosylation of IRE1α (Fig. 3e, f). These data, then, confirm the crucial role of iNOS in the pathogenesis of HFpEF and in regulation of the IRE1α-Xbp1s axis in heart.

To test whether pharmacological inhibition of iNOS ameliorates cardiac relaxation and exercise intolerance in HFpEF, we exposed 5-week HFD+L-NAME mice to L-N6-(1-iminoethyl)lysine (L-NIL), a specific inhibitor of iNOS[17] (Extended Data Fig. 10a). After three days of L-NIL treatment, the iNOS inhibitor decreased NO metabolites in HFD+L-NAME mouse urine as compared with animals treated with vehicle (Extended Data Fig. 10b). In the absence of significant changes in LVEF% (Extended Data Fig. 10c), blood pressure (Extended Data Fig. 10d, e), L-NIL administration partially improved ventricular relaxation (Extended Data Fig. 10f, g) and exercise performance (Extended Data Fig. 10h) in HFD+L-NAME mice. Interestingly, these observations in HFD+L-NAME L-NIL-treated animals occurred in the absence of concomitant restoration of Xbp1s transcript levels (Extended Data Fig. 10i). Different from iNOS genetic deletion, in which long-term reduction of iNOS activity prevents the aberrant S-nitrosylation of IRE1α, restoring Xbp1s levels in the myocardium, the amelioration of LV diastolic properties and exercise tolerance induced by short-term iNOS inhibition appears to be independent of myocardial Xbp1s levels, suggesting additional beneficial mechanisms of iNOS inhibition on cardiac relaxation.

Discussion

HFpEF is a lethal disorder for which there are no effective clinical therapies. Given the limitations of current preclinical models, we developed a novel murine model of HFpEF that recapitulates the vast majority of the clinical features of the syndrome. The interventions we used to replicate the clinical phenotype are based on the (limited) pathophysiological observations available from the human condition; alterations in NO pathway(s) have been repeatedly observed in human HFpEF hearts, and our model seizes upon this fact to manipulate NO biology from the start. By contrast, only limited evidence is available to implicate the renin-angiotensin-aldosterone system (RAAS) axis in HFpEF, which may

explain why preclinical models based on RAAS manipulation elicit only a limited number of HFpEF features, and therapies targeting RAAS have failed in clinical trials. Using multiple approaches in preclinical models of HFpEF and human myocardial samples from HF subjects, we uncovered evidence implicating systemic inflammation, iNOS activation, nitrosative stress, and suppression of the IRE1α-Xbp1s arm of the UPR. Indeed, our findings implicate meta-inflammation and its master mediator, iNOS, as critical elements in the pathophysiology of HFpEF.

Current treatments of HFpEF that have focused on increasing NO bioavailability have reported neutral[18–20] or negative results[21,22]. Our findings, indeed, provide a biological explanation for the failure of NO-inducing approaches as therapeutic strategies. Therefore, turning attention to strategies focusing on reducing iNOS activation and other pro-inflammatory mediators, as well as to novel molecular mediators of nitrosative stress, such as components of iNOS/S-nitrosylase complex[23], may hold promise in HFpEF.

Working from the realities of clinical HFpEF, including multi-organ co-morbidities, we have developed a novel murine model of HFpEF that recapitulates the myriad features of the syndrome. Further, we have uncovered iNOS-dependent regulation of IRE1α-Xbp1s as a pathophysiological driver of the syndrome.

Methods

Experimental animals

All experiments involving animals conformed to the Guide for the Care and Use of Laboratory Animals published by the US National Institutes of Health (NIH Publication 8th edition, update 2011) and were approved by the Institutional Animal Care and Use Committee of the University of Texas Southwestern Medical Center. The studies were in compliance with all ethical regulations. C57BL/6N mice were used for wild-type (WT) studies. Tetracycline responsive elements (TRE)-Xbp1s mice were crossed with mice harbouring tetracycline transactivator (tTA) transcription factor driven by α-myosin heavy chain promoter (αMHC-tTA) to generate mice with cardiomyocyte-specific inducible overexpression of Xbp1s (Xbp1s TG) as previously described[10]. iNOS knockout mice (*Nos2*$^{-/-}$, B6.129P2-Nos2tm1Lau/J) were purchased from Jackson Laboratory (Bar Harbor, Maine) to establish an in-house colony. ZSF1-obese (ZSF1-LeprfaLeprcp/Crl, strain code 378) and Wistar-Kyoto (WKY) rats were obtained from Charles River Laboratories (Wilmington, Massachusetts). Male adult (8/12 week-old) mice were used in the experiments. Analyses in rats were carried out when the animals reached 20 weeks of age. Mice and rats were maintained on a 12-hour light/dark cycle from 6 AM to 6 PM and had unrestricted access to food (#2916, Teklad for CHOW groups and D12492, Research Diet Inc. for the HFD groups) and water. N$^{[w]}$-nitro-l-arginine methyl ester (L-NAME; 0.5 g/L, Sigma Aldrich) was supplied in the drinking water for the indicated periods of time, after adjusting the pH to 7.4. L-N6-(1-iminoethyl)lysine (L-NIL, Cayman Chemical) was administered intraperitoneally (i.p.) at a dose of 80 mg/kg body weight twice a day for three days. Transverse aortic constriction (TAC or severe TAC, sTAC) was surgically induced as previously described[24].

Conventional echocardiography and Doppler imaging

Transthoracic echocardiography was performed using a VisualSonics Vevo 2100 system equipped with MS400 transducer (Visual Sonics Inc). Left ventricular ejection fraction and other indices of systolic function were obtained from short axis M-mode scans at the mid-ventricular level, as indicated by the presence of papillary muscles, in conscious, gently restrained mice. Apical 4-chamber views were used in anesthetized mice to obtain diastolic function measurements using pulsed-wave and tissue Doppler at the level of mitral valve. Anesthesia was induced by 5% isoflurane and confirmed by lack of response to firm pressure on one of the hind paws. During echocardiogram acquisition, under body temperature-controlled conditions, isofluorane was reduced to 1.0–1.5% and adjusted to maintain heart rate in the range of 415–460 beats per minute. Parameters collected include: heart rate (HR), left ventricular end-diastolic diameter (LVID,d), left ventricular end-systolic diameter (LVID,s), end-diastolic interventricular septal wall thickness (IVS,d), left ventricular end-diastolic posterior wall (LVPW,d), left ventricular fractional shortening (LVFS), left ventricular ejection fraction (LVEF), peak Doppler blood inflow velocity across the mitral valve during early diastole (E), peak Doppler blood inflow velocity across the mitral valve during late diastole (A), isovolumic relaxation time (IVRT), peak tissue Doppler of myocardial relaxation velocity at the mitral valve annulus during early diastole (E'), and early filling deceleration time (DT). At the end of the procedures all mice recovered from anesthesia without difficulties. All parameters were measured at least 3 times, and averages are presented.

Speckle tracking echocardiography and strain analysis

B-mode traces acquired from the parasternal long-axis view were used to calculate global strain in longitudinal dimensions using VevoStrain software (Visual Sonics Inc.) and a speckle-tracking algorithm. Velocity and displacement were also calculated in both the long- and short-axes. Values generated by strain analysis in the longitudinal dimension are negative, indicative of fiber shortening. B-mode images were selected based on quality (high frame rates) and on the ability to visualize both the endocardial and epicardial LV wall borders. Borders of the endocardium and epicardium were traced, and semi-automated strain analysis was performed. Average peak global strain values were obtained from six independent anatomical segments of the LV.

Coronary flow reserve

Coronary flow velocity was measured in cine traces of the left proximal coronary artery using pulsed-wave Doppler at baseline and under hyperemic conditions induced by inhalation of 1.5% and 3.0% isoflurane, respectively. Coronary flow reserve (CFR) is expressed as the ratio of peak blood flow velocity during hyperemia and peak blood flow velocity at baseline.

Tail cuff blood pressure recordings

Systolic blood pressure was measured noninvasively in conscious mice using the tail-cuff method and a CODA instrument (Kent Scientific). Animals were placed in individual holders on a temperature-controlled platform (37°C), and recordings were performed under

steady-state conditions. Before testing, all mice were trained to become accustomed to short-term restraint. Blood pressure was recorded for at least 4 consecutive days and readings were averaged from at least 8 measurements per session

Pulse wave velocity

Pulse wave velocity (PWV) was measured noninvasively over the entire aorta. Pulsed Doppler images were obtained at the ascending aorta (immediately cranial to the aortic valve) and the abdominal aorta (immediately cranial to the iliac bifurcation). Subsequently, the distance between the two locations was approximated by an external body tape measurement. PWV was calculated as the ratio of ΔX and ΔT ($PWV=\Delta X/\Delta T$), where ΔX is the distance between the two anatomical locations where the Doppler signals were recorded and ΔT is the electrocardiography (ECG)-based transit time between averaged waveforms at both locations.

Pressure-volume analysis

An apical approach was used to obtain invasive pressure-volume measurements from anesthetized (pentobarbital sodium 40–50 mg/kg) mice using a mouse 1.4-F catheter with pressure and conductance sensors (SPR 839, Millar Instruments, Houston, TX) as previously described[25]. The inferior vena cava was located and occluded during a pause in ventilation to acquire load-independent indices. Data were analyzed using PV Lab Chart software (version 8).

Exercise exhaustion test

After 3 days of acclimatization to treadmill exercise, an exhaustion test was performed in the experimental groups of mice. Animals ran uphill (20°) on the treadmill (Columbus Instruments) starting at a warm-up speed of 5 m/min for 4 min after which speed was increased to 14 m/min for 2 min. Every subsequent 2 min, the speed was increased by 2 m/min until the animal was exhausted. Exhaustion was defined as the inability of the animal to return to running within 10 sec of direct contact with an electric-stimulus grid. Running time was measured and running distance calculated.

Grip strength test

Muscle strength was assessed by a grip strength test performed by the Neuro-Models Core Facility at UT Southwestern Medical Center. Mice from different experimental groups were horizontally drawn along a straight line (to avoid the effect of body weight differences) and allowed to grasp a pull-bar assembly connected to the grip-strength meter (Columbus Instruments). Mice were then gently pulled by the tail away from the sensor until the grasp was broken, and peak force in grams was recorded. The test was considered complete when 6 trials per limb pair (5 forelimb, 5 hindlimb) were recorded. All measurements were performed by the operator in a blinded fashion.

Intraperitoneal glucose tolerance test

Intraperitoneal glucose tolerance test were performed by injection of glucose (2 g/kg in saline) after 6-hour fasting. Tail blood glucose levels [mg/dL] were measured with a glucometer before (0 min) and at 15, 30, 45, 60 and 120 min after glucose administration.

Histology

Hearts and skeletal muscles (soleus and gastrocnemius/plantaris) were harvested and either flash frozen in embedding medium containing a 3:1 mixture of Tissue Freezing Medium (Triangle Biomedical Sciences, Durham, NC) and gum tragacanth (Sigma, St. Louis, MO) or fixed in 4% paraformaldehyde (PFA) overnight and processed for routine paraffin histology (5 μm sections stained with hematoxylin and eosin, Masson's trichrome or Picrosirius red). Frozen sections were cut on a cryotome and stained for ATPase activity as previously described[26]. Wheat germ agglutinin (WGA) staining and lectin staining were used to measure cardiomyocyte cross-sectional area (CSA) and to quantify capillary density, respectively. After deparaffinization and antigen retrieval with hot citrate buffer (Antigen Retrival Citra, BioGenex), slides were incubated with WGA conjugated to Alexa Fluor® 488 (50 mg/mL, 1 h, room temperature) or with biotin conjugate lectin from *Griffonia simplicifolia* (overnight, 4°C). Cardiomyocyte size, fibrosis area and capillary numbers were visualized with Leica DM2000 upright photomicroscope and quantified using ImageJ software version 2.0 (three microscopic fields per heart). For immunofluorescence studies, cardiac sections were permeabilized with 0.3% Triton-phosphate buffer saline (PBS), blocked with 5% Goat serum-PBS and then incubated with KDEL (#ADI-SPA-827-D, Enzo Life Sciences) antibody 1:200 in 3% bovine serum albumin (BSA) in PBS overnight at 4°C. After washing, sections were incubated with the anti-mouse secondary antibody conjugated to Alexa Fluor® 488 (1:500 in 3% BSA-PBS, 1 h at RT). Sections were then mounted using anti-fade reagent supplemented with DAPI (Invitrogen) and images were obtained using a Zeiss LSM 880 upright confocal fluorescence microscope.

Isolated muscle preparation and stimulation

Muscle preparation was accomplished as described previously[27]. Briefly, soleus muscles were isolated surgically from mice fed CHOW or HFD+L-NAME and mounted on Grass FT03.C force transducers connected to a Powerlab 8/SP data acquisition unit (AD Instruments, Colorado Springs, CO), bathed in physiological salt solution at 37°C, and gassed continuously with 95% O_2-5% CO_2. After calibration, muscles were adjusted to their initial lengths at a point in which the passive force is 0.5 g and were stimulated with two platinum wire electrodes to establish the optimal length (Lo). Muscles were then stimulated at 150 Hz in 2 sec bursts until the maximal tetanic contraction was achieved. Stress (mN/mm^2) was calculated to normalize contraction responses to tissue cross-sectional areas. For evaluation of relaxation, muscles were stimulated at 150 Hz for 40 sec. Values were expressed as percentage of the force during the protocol relative to peak force.

Cardiomyocyte isolation and treatment

Adult mouse ventricular myocytes (AMVMs) were isolated from littermates of each experimental group. Briefly, hearts were isolated and immediately digested through

retrograde perfusion with perfusion buffer (113 mM NaCl, 4.7 mM KCl, 0.6 mM KH_2PO_4, 0.6 mM Na_2HPO_4, 1.2 $MgSO_4$, 10 mM HEPES, 12 mM $NaHCO_3$, 10 mM$KHC0_3$, 30 mM Taurine, 10mM BDM, 5.5 mM glucose) for one min followed by buffer containing liberase-TM (0.025 mg/mL, Roche) and trypsin (0.025%) for 14 min. The left ventricle was dissected and minced in perfusion medium supplemented with 10% dialyzed FBS. After filtration, AMVMs were allowed to sediment by gravity and non-cardiomyocytes were discarded. Calcium reintroduction was performed stepwise from 0–1.8 mM in 6 steps. Neonatal rat ventricular myocytes (NRVMs) were isolated from 1–2 day old Sprague-Dawley rat pups as previously described[10]. Cell preparations typically contained greater than 95% cardiomyocytes. When appropriate, tunicamycin from *Streptomyces sp.* (Sigma-Aldrich, 1 μg/mL for 24 h) was employed.

Sarcomere length measurements in paced cardiomyocytes

Sarcomere shortening and relaxation were measured in freshly isolated AMVMs using the integrated IonOptix LLC contractility/photometry system. Briefly, AMVMs were electrically stimulated at 0.5 Hz using a field stimulator and changes in sarcomeric length recorded. Basal and peak sarcomere length, maximum departure/return velocities and time to peak were measured. All measurements were performed at room temperature.

Adenovirus production, purification and transduction

Mouse iNOS cDNA was obtained from Addgene (#19295) and subcloned into an adenovirus expression vector using Adeno-X™ Adenoviral System 3 (CMV promoter and Zsgreen1 reporter, Takara) following the manufacturer's instructions. Adeno-X 293 cell line was purchased from Clontech (Adeno-X™ 293 Cell Line, cat# 632271). The cell line was authenticated by the vendor and Mycoplasma detection was tested negative. Adenoviruses were harvested from culture supernatant and cell lysates and the viral titer was determined. NRVMs were transduced with increasing multiplicity of infection (MOI) of virus and cells were harvested 24-hour post-infection. An α-galactosidase adenovirus (AdLacZ) construct contained in the kit was used as control at the same MOI. Adenoviruses carrying wild-type (WT) human IRE1α and IRE1α harboring mutations in two target nitrosylation sites in the RNase domain (IRE1-M1+M2) were kindly donated from Gökhan S. Hotamisligil MD PhD (Harvard University) and Ling Yang PhD (University of Iowa).

RNA isolation and qPCR

Total RNA was extracted from murine and rat hearts, AMVMs, or NRVMs using TRIzol reagent or Quick-RNA™ MicroPrep kit (Zymo Reaserch). A total of 500 ng RNA was used for reverse transcription using iScript reagent (Bio-Rad). qPCR reactions were performed in triplicate with SYBR master mix (Bio-Rad). For human hearts, total RNA was extracted using the miRNeasy Mini Kit (Qiagen) then reverse transcribed into cDNA using the High Capacity cDNA Reverse Transcription Kit (Applied Biosystems). Real time PCR was performed in duplicate using TaqMan Gene Expression Assay probes with specific primers for target sequences. The $2^{-\Delta\Delta CT}$ relative quantification method, using *18S* or *GAPDH* for normalization, was used to estimate the amount of target mRNA in samples, and fold ratios were calculated relative to mRNA expressions levels from control samples. The following PCR primers sequences were used (forward, reverse):

Xbp1s-mouse/rat (GGTCTGCTGAGTCCGCAGCAGG, GAAAGGGAGGCTGGTAAGGAAC); *Bip-mouse* (CATGGTTCTCACTAAAATGAAAGG, GCTGGTACAGTAACAACTG);

ATF6-mouse (AGAAAGCCCGCATTCTCCAG, ACTCCCAGAATTCCTACTGATGC);

ATF4-mouse (ATGGCCGGCTATGGATGAT, CGAAGTCAAACTCTTTCAGATCCATT);

CHOP-mouse (CTGCCTTTCACCTTGGAGAC, CGTTTCCTGGGGATGAGATA);

NOS2-mouse (GTTCTCAGCCCAACAATACAAGA, GTGGACGGGTCGATGTCAC);

NOS3-mouse (TCAGCCATCACAGTGTTCCC, ATAGCCCGCATAGCGTATCAG);

NPPA-mouse (CTGGGACCCCTCCGATAGAT, TTCGGTACCGGAAGCTGTTG);

NPPB-mouse (TTTGGGCTGTAACGCACTGAA, TGTGGCAAGTTTGTGCTCCA);

MyHC-1-mouse (CCTTGGCACCAATGTCCCGGCTC, GAAGCGCAATGCAGAGTCGGTG);

MyHC-2A-mouse (ATGAGCTCCGACGCCGAG, TCTGTTAGCATGAACTGGTAGGCG);

MyHC-2X-mouse (AAGGAGCAGGACACCAGCGCCCA, ATCTCTTTGGTCACTTTCCTGCT);

TNFα-mouse (ATCGGTCCCCAAAGGGATGA, GGTGGTTTGCTACGACGTG);

IL1β-mouse (TAACTGCACCCACTTCCCAG, AGGCTTGGCAACCCAAGTAA);

IL6-mouse (CTCTGCAAGAGACTTCCATCCA, GACAGGTCTGTTGGGAGTGG);

18S-mouse/rat (AAACGGCTACCACATCCAAG, CCTCCAATGGATCCTCGTTA);

Xbp1s-human (CTGAGTCCGCAGCAGGTG, GTCCAGAATGCCCAACAGGA);

Xbp1u-human (CGGAAGCCAAGGGGAATGAA, TGTTCTGGAGGGGTGACAAC);

*NOS2-human (*TCCCGAAGTTCTCAAGGCAC, TTCTTCACTGTGGGGCTTGC);

GAPDH-human (TCAACGACCACTTTGTCAAGCTCA, GCTGGTGGTCCAGGGGTCTTACT)

Electrophoretic analysis of Xbp1 splicing

Xbp1 splicing was assessed as previously described[28]. Briefly, cDNAs from mouse and rat hearts were subjected to semiquantitative PCR using the following primers (5′-CCTTGTGGTTGAGAACCAGG-3′ and 5′-CTAGAGGCTTGGTGTATAC-3′) to amplify a 451–base pair (bp) unspliced Xbp1 fragment or a 425-bp spliced Xbp1 fragment respectively. PCR products were then subjected to *Pst* I restriction enzyme digestion, which only cleaves the intron included in the unspliced Xbp1 cDNA to yield a 154-bp and a 297-bp

fragment, leaving the spliced Xbp1 cDNA intact. 18S transcript was also amplified as internal control and the PstI–digested products were analyzed by 2% agarose gel electrophoresis.

Immunoblot analysis

Protein extracts from frozen mouse, rat, and human hearts, AMVMs and NRVMs were prepared by lysis in ice-cold modified RIPA buffer (150 mM NaCl, 50 mM Tris HCL pH 7.4, 1% Triton-X 100, 0.5% sodium deoxycholate, 0.1% SDS, 5 mM EDTA, 2 mM EDTA) containing protease and phosphatase inhibitors. Proteins were separated by SDS-PAGE on 4%–20% gradient gels (Bio-Rad) and transferred to nitrocellulose membranes. An Odyssey scanner (LI-COR version 3.0) was used as detection system. For human myocardial samples, protein lysates were prepared using cell lysis buffer (CST, Cell Signaling Technology) with the addition of 1mM phenylmethylsulfonyl fluoride (PMSF). Lysates were prepared using the Retsch Mixer Mill. Capillary-based immunoassay was performed using the Wes-Simple Western method with the anti-rabbit detection module (ProteinSimple). Protein expression was measured by chemiluminescence and quantified as area under the curve using the Compass for Simple Western program (ProteinSimple). Proteins were detected with the following primary antibodies: pIRE1α [Ser724] (NB100–2323, Novus Biological); IRE1α (#3294, Cell Signaling), GRP78 (#3177, Cell Signaling); anti-GRP94 (#2104, Cell Signaling); PERK (#3192, Cell Signaling); ATF6 (24169–1-AP, Proteintech); iNOS (#13120, Cell Signaling); nNOS (#4234, Cell Signaling); eNOS (#9572, Cell Signaling); GAPDH (10R-G109a, Fitzgerald).

Cytokines/chemokines analyses using antibody array membrane

RayBio® C-Series mouse cytokine antibody array C1 (AAM-CYT-1–8) was used according to the manufacturer instructions. Briefly, the membranes were placed in the plastic tray provided in the kit, and then 200 μL of plasma from CHOW and HFD+L-NAME groups was incubated overnight in the designated well at 4°C. Subsequently, the samples were aspirated, the membranes were washed with wash buffer and then incubated with 1 mL of biotinylated antibody cocktail overnight at 4°C. After washing, membranes were incubated with HRP-Streptavidin overnight at 4°C. Detection buffer was used to develop a chemiluminescent signal and the LI-COR instrument was used to detect signal intensity

Measurement of nitrite and nitrate

The amounts of nitrite and nitrate, the breakdown products of nitric oxide, were measured in urine samples or cell media with the Nitrate/Nitrite colorimetric assay kit (Cayman Chemicals) according to the manufacturer's instructions.

Lactate dehydrogenase (LDH) assay

To evaluate cell survival, LDH release was quantified using the CytoTox96 cytotoxicity kit (Promega) according to the manufacturer's instructions. Each experiments was performed in three biological replicates each time in triplicate. LDH release was calculated as follows: (medium LDH)/(medium LDH + intracellular LDH).

Determination of S-nitrosylation

Hearts were excised, snap-frozen in liquid nitrogen, and stored at −80ºC until homogenization. Cardiac tissue or NRVMs samples were homogenized in lysis buffer (phosphate buffered saline supplemented with 10% glycerol, 1 mM EDTA, 1mM EGTA, 1% Triton X-100, protease/phosphatase inhibitors and 0.1 mM neocuproine). Lysates were spun at 10,000*xg* and supernatants were used for protein determination using the BCA method (Thermo Fisher Scientific). Free cysteines were blocked at room temperature in HENS buffer (100 mM HEPES (pH 7.0), 1 mM EDTA, 0.1 mM neocuproine, and 2.5% SDS) using 100 mM N-ethylmaleimide (NEM). Proteins were acetone-precipitated, and pellets washed using methanol. The protein pellet was resuspended in HENS buffer (100 mM Hepes, 1% SDS, 1 mM EDTA, 0.1 mM neocuproine) pH 8.0 and labeled using 40 mM ascorbic acid and 0.4 mM Tandem Mass Tag (TMT; Thermo Fisher Scientific). A negative control without ascorbic acid and a positive control with 1 mM S-nitrosoglutathione (GSNO) were included. Immunoprecipitation was carried out using 500 μg labeled protein and 5 μL IRE1α antibody and 25 μL Dynabeads Protein G in IP buffer (overnight, 4ºC). Beads were magnetically separated and washed 5 times with IP buffer and then eluted using a 2x Laemmli buffer. For some experiments, S-nitrosylated proteins were separated using resin assisted capture protocols (SNO-RAC). Total lysates (2 mg) were blocked twice with 100mM NEM in HENS buffer pH 7.0 at 55º C for 30 min to ensure complete cysteine blockage. Proteins were acetone precipitated and washed with methanol to remove unreacted NEM. Then, samples were incubated with freshly prepared 50 mM ascorbate and 55 mg thiopropyl-sepharose and rotated end-over-end in the dark for 4 h. The bound SNO proteins were washed with HEN/1% SDS for five times; SNO proteins were then eluted with Laemmli sample buffer supplemented with 5% β-mercaptoethanol and analyzed by SDS-PAGE and Western blot.

Human myocardial tissue

Human myocardial tissue samples were collected under protocols approved by Institutional Review Board (IRB) at Johns Hopkins University (Maryland, USA) and consent for biopsy procedures or use of explanted tissues prospectively obtained in all cases. HFpEF patients were referred for cardiac catheterization and right ventricular endomyocardial biopsy due to clinical suspicion of infiltrative cardiomyopathy. HFrEF samples were obtained from the right ventricular septum of explanted dilated failing hearts prior to orthotopic heart transplantation. Control samples were obtained from the right ventricular septum of nonfailing explanted unused donor hearts. Control and HFrEF samples were provided by collaborators at the Perelman School of Medicine at the University of Pennsylvania (Philadelphia, Pennsylvania, USA) through an IRB-approved protocol.

Statistical analysis

Results are presented as mean ± S.E.M. Differences were analyzed by two-tailed unpaired Student's *t*-test for experiments with 2 groups and one-way or two-way analysis of variance (ANOVA) plus Sidak's *post hoc* test for multiple comparisons as appropriate in experiments including ≥3 groups. A minimum value of $p<0.05$ was considered statistically significant. All experiments were performed with at least three biological replicates. Statistical analyses

were conducted using GraphPad Prism software 8.0 or SPSS Statistics version 19 (SPSS Inc., Chicago, IL) for the comparison of categorical variables in the Extended Data Table 2. No statistical analysis was used to predetermine sample sizes; estimates were made based on our previous experience, experimental approach, availability and feasibility required to obtain statistically significant results. Experimental animals were randomly assigned to each experimental/control group. Investigators were blinded to the genotypes of the individual animals during the experiments and outcome assessments.

Extended Data

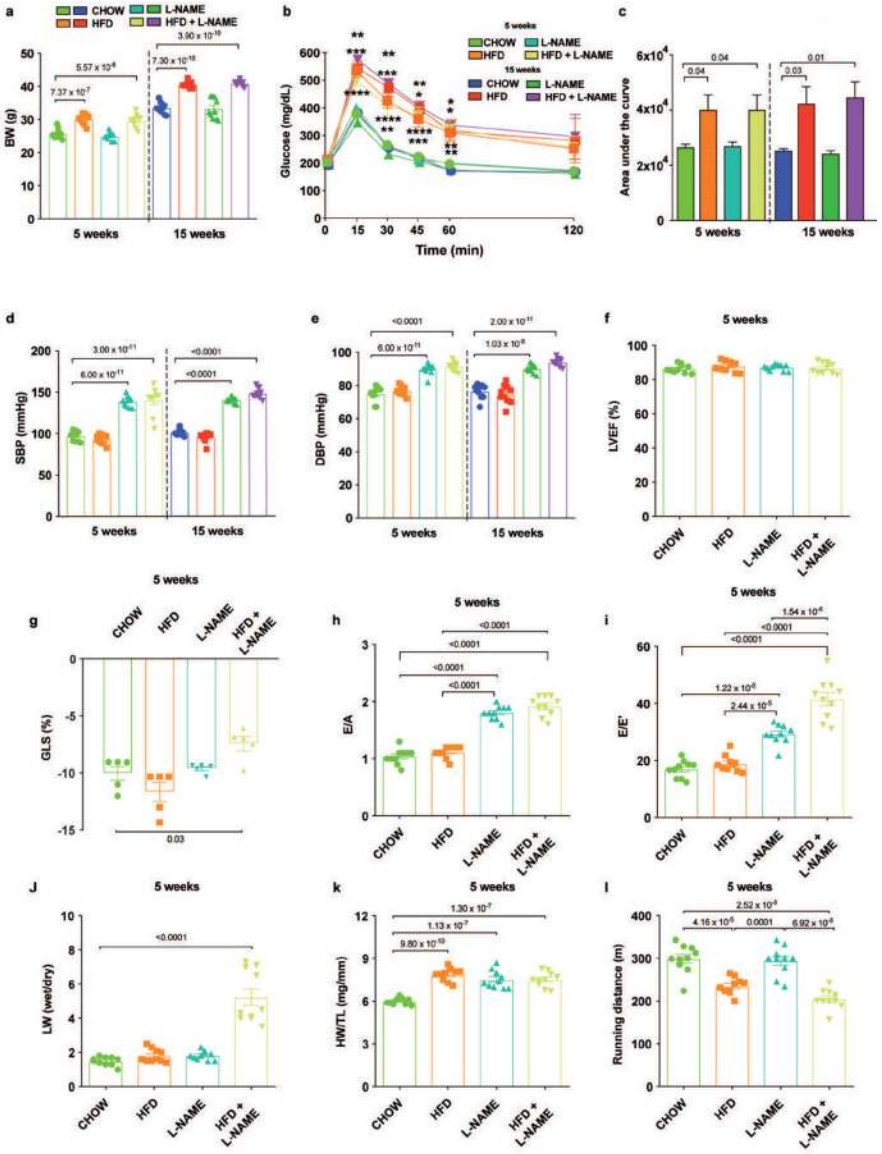

Extended Data Figure 1. Systemic and cardiac phenotype of mice after five or fifteen weeks of different dietary regimens.

a, Body weight (BW) of mice of different experimental groups after five or fifteen weeks of diet (n=10 mice per group for each time point). **b**, Intraperitoneal glucose tolerance test (ipGTT) after five or fifteen weeks of diet (for five weeks n=10 mice per group; for fifteen weeks n=5 mice per group). **c**, Bar graphs depicting the area under the curve of the 5- and 15-week time points ipGTT experiment (for five weeks n=10 mice per group; for fifteen weeks n=5 mice per group). **d**, Systolic blood pressure (SBP) and **e**, diastolic blood pressure (DBP) of different experimental groups after five or fifteen weeks of treatment (n=10 mice per group for each time point). **f**, Percent left ventricular ejection fraction (LVEF%), **g**, LV global longitudinal strain (GLS), **h**, Ratio between mitral E wave and A wave (E/A), **i**, Ratio between mitral E wave and E' wave (E/E'), **j**, Ratio between wet and dry lung weight (LW), **k**, Ratio between heart weight and tibia length (HW/TL) and **l**, Runninng distance during exercise exhaustion test of mice after five weeks of diet (for LVEF%, E/A ratio, E/E' ratio,

HW/TL ratio, running distance and LW wet/LW dry ratio n=10 mice per group. For LV GLS n=5 mice per group). Results are presented as mean±S.E.M. **a, c-l** One-way ANOVA followed by Sidak's multiple comparisons test. **b**, Two-way ANOVA followed by Sidak's multiple comparisons test. **a, c-l** Numbers above square brackets show significant *P* values. **b, for five weeks** 15' ***P=0.0003 CHOW vs. HFD, ***P=0.0004 CHOW vs. HFD+L-NAME; 30' ***P=0.0008 CHOW vs. HFD, **P=0.006 CHOW vs. HFD+L-NAME; 45' *P=0.010 CHOW vs. HFD, ***P=0.0008 CHOW vs. HFD+L-NAME; 60' *P=0.049 CHOW vs. HFD, **P=0.0096 CHOW vs. HFD+L-NAME. **for fifteen weeks**, 15' **P=0.008 CHOW vs. HFD, ****P<0.0001 CHOW vs. HFD+L-NAME; 30' **P=0.005 CHOW vs. HFD, ****P<0.0001 CHOW vs. HFD+L-NAME; 45' **P=0.009 CHOW vs. HFD, ****P<0.0001 CHOW vs. HFD+L-NAME; 60' *P=0.028 CHOW vs. HFD, **P=0.0020 CHOW vs. HFD+L-NAME.

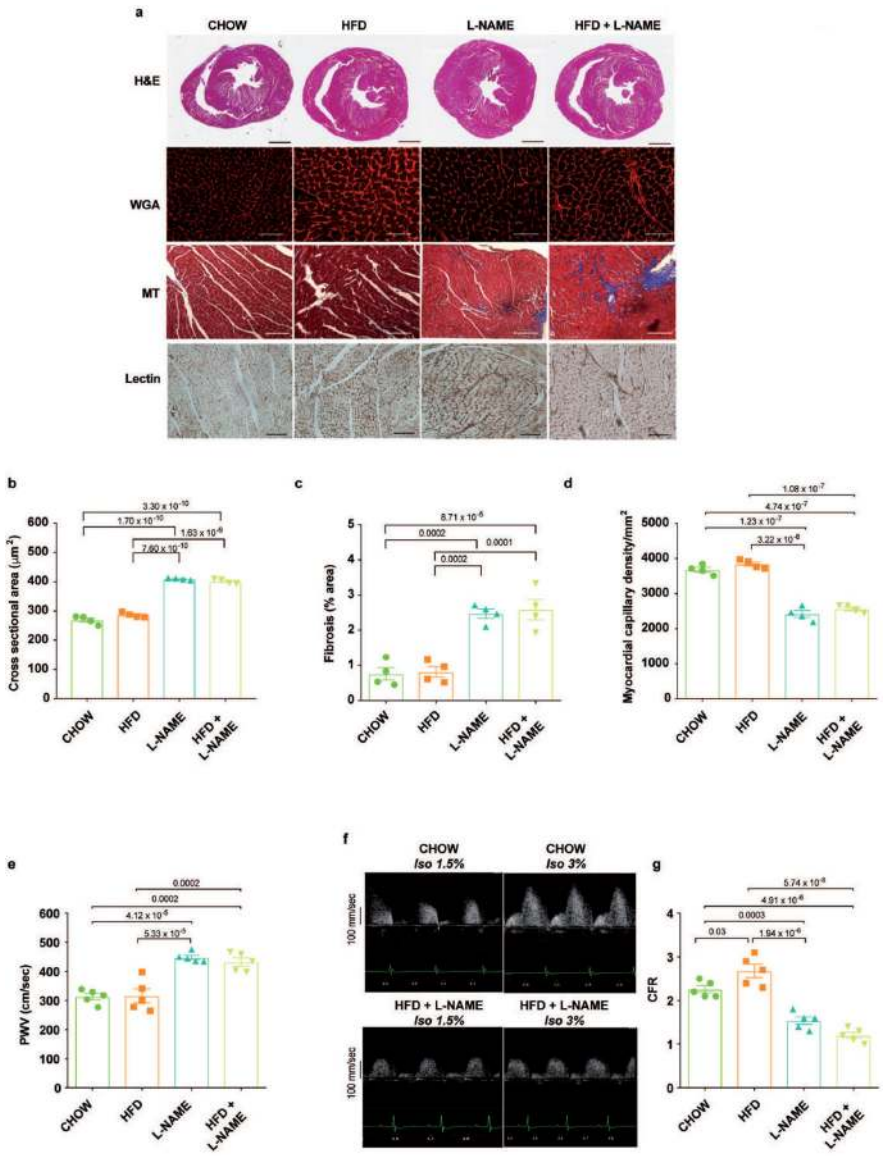

Extended Data Figure 2. Heart morphology and vascular characterization of mice after five weeks of different dietary regimens.

a, Representative images of hematoxylin & eosin (H&E), wheat germ agglutinin (WGA), Masson's Trichrome (MT) and lectin staining in transversal sections of left ventricle of mice of different experimental groups. Images are representative of four independently performed experiments with similar results. Scale bars: 500 μm for H&E; Scale bars: 50 μm for WGA, MT and lectin. **b**, WGA quantification of cardiomyocyte cross sectional area (n=4 mice per group). **c**, Percentage of fibrosis area of MT-stained transversal sections (n=4 mice per group). **d**, Myocardial capillary density (n=4 mice per group). **e**, Aortic pulse wave velocity (PWV) of mice of different experimental groups (n=5 mice per group). **f**, Representative pulse wave Doppler tracings of coronary flow in CHOW (top panels) and HFD+L-NAME (bottom panels) mice under basal condition (left panels – Isofluorane, Iso 1.5%) and after hyperemic stimulus (right panels – Iso 3%). Images are representative of five independent mice. **g**, Coronary flow reserve (CFR) quantification (n=5 mice per group). Results are

presented as mean±S.E.M. **b-d, e, g** One-way ANOVA followed by Sidak's multiple comparisons test. Numbers above square brackets show significant *P* values.

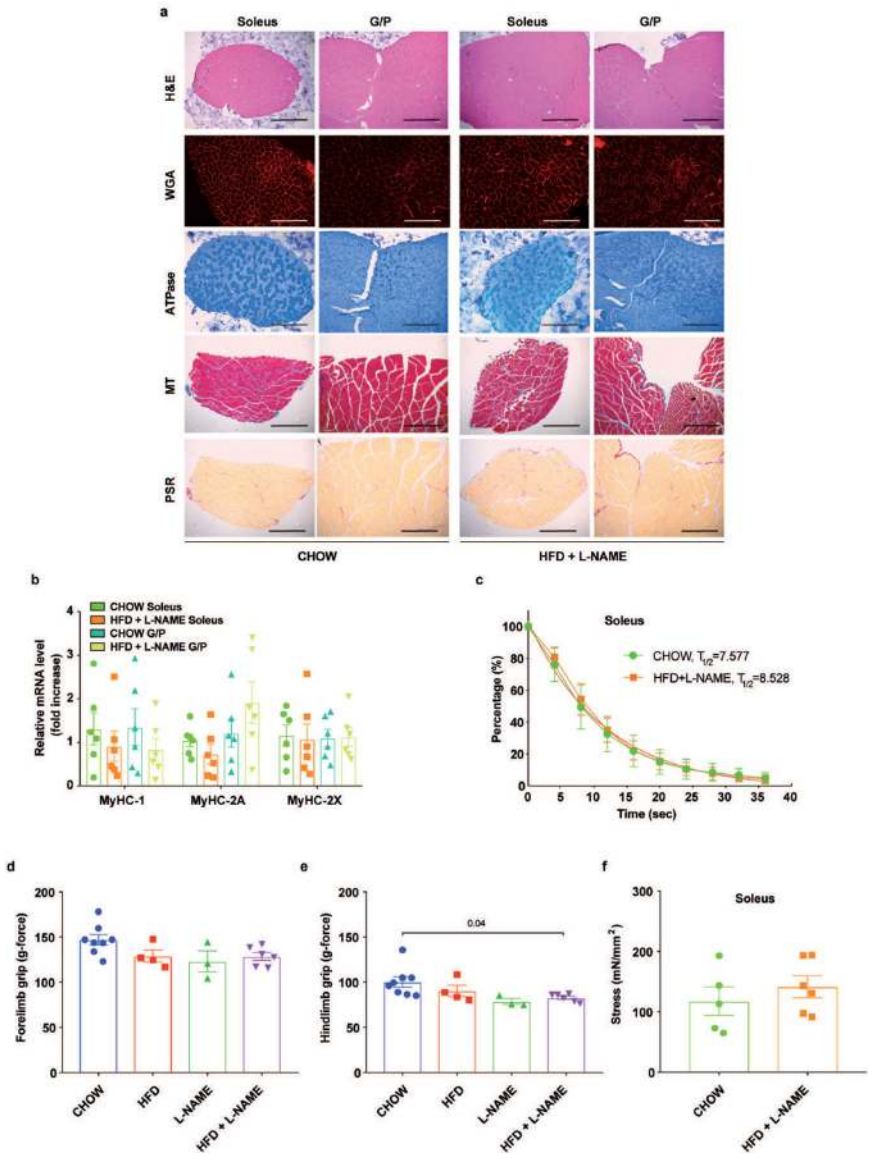

Extended Data Figure 3. Histological and functional analyses of skeletal muscle in mice after five weeks of different dietary regimens.

a, Representative images of hematoxylin & eosin (H&E), wheat germ agglutinin (WGA), metachromatic ATPase (ATPase), Masson's Trichrome (MT) and Picrosirius red (PSR) staining of soleus and gastrocnemius/plantaris (G/P) from CHOW and HFD+L-NAME mice. Images are representative of three independently performed experiments with similar results. Scale bars: 50 μm. **b**, mRNA level of myosin isoforms (MyHC-1, MyHC-2A, MyHC-2X) of soleus and G/P from CHOW and HFD+L-NAME mice (n=5 mice per group). **c**, Relaxation curve of isolated soleus from CHOW and HFD+L-NAME mice (n=5 mice per CHOW group; n=6 mice per HFD+L-NAME group). *In vivo* forelimb **d**, hindlimb **e**, and grip force measurements of mice of different experimental groups (n=8 mice per CHOW group; n=4 mice per HFD group; n=3 mice per L-NAME group; n=6 mice per HFD+L-NAME group). **f**, Maximal tetanic stresses in soleus from CHOW and HFD+L-NAME mice (n=5 mice per CHOW group; n=6 mice per HFD+L-NAME group). Results are presented as mean±S.E.M.

b, c, f Two-tailed unpaired Student's *t*-test (CHOW vs. HFD+L-NAME soleus; CHOW vs. HFD+L-NAME G/P). **d, e** One-way ANOVA followed by Sidak's multiple comparisons test. Numbers above square brackets show significant *P* values.

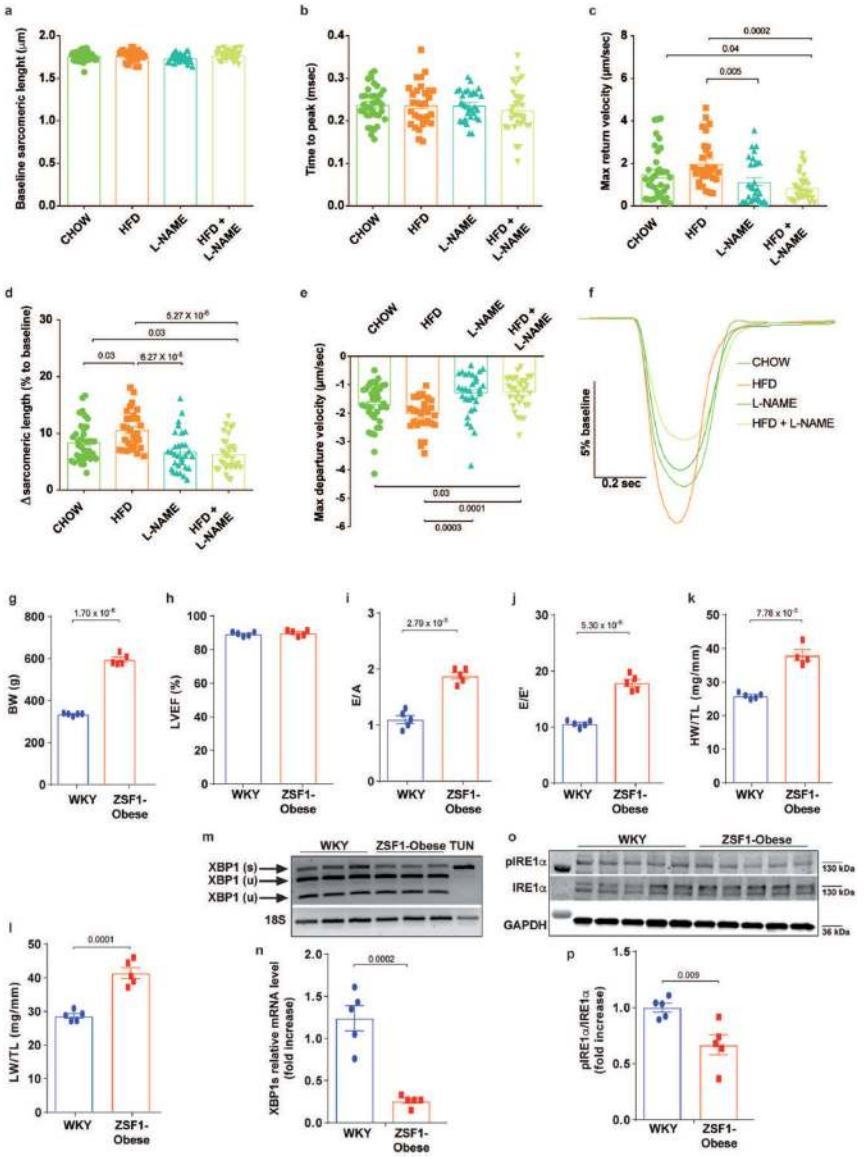

Extended Data Figure 4. Adult mouse ventricular cardiomyocyte contractility after five weeks of different dietary regimens and functional characterization and IRE1α-Xbp1s axis in ZSF1-Obese rats at twenty weeks of age.

a, Baseline sarcomeric length (n=4 mice and n=35 cells per CHOW group; n=3 mice and n=30 cells per HFD group; n=3 mice and n=30 cells per L-NAME group; n=3 mice and n=31 cells per HFD+L-NAME group). **b**, Time to peak (n=4 mice and n=36 cells per CHOW group; n=3 mice and n=30 cells per HFD group; n=3 mice and n=30 cells per L-NAME group; n=3 mice and n=31 cells per HFD+L-NAME group). **c**, Maximum return velocity (n=4 mice and n=36 cells per CHOW group; n=3 mice and n=29 cells per HFD group; n=3 mice and n=30 cells per L-NAME group; n=3 mice and n=31 cells per HFD+L-NAME group). **d**, Change (Δ) in sarcomeric length related to baseline (n=4 mice and n=36 cells per CHOW group; n=3 mice and n=30 cells per HFD group; n=3 mice and n=30 cells per L-NAME group; n=3 mice and n=31 cells per HFD+L-NAME group). **e**, Maximum departure velocity (n=4 mice and n=35 cells per CHOW group; n=3 mice and n=30 cells per

HFD group; n=3 mice and n=29 cells per L-NAME group; n=3 mice and n=28 cells per HFD+L-NAME group). **f**, Representative tracings of cardiomyocyte contraction/relaxation during pacing. Each trace depicts one cell representative of the average for each experimental group. **g**, Body weigth (BW), **h**, Percent left ventricular ejection fraction (LVEF%), **i**, Ratio between mitral E wave and A wave (E/A), **j**, Ratio between mitral E wave and E' wave (E/E'), **k**, Ratio between heart weight and tibia length (HW/TL) ratio, and **l**, Lung weight (LW)/TL ratio of 20-week old Wistar Kyoto (WKY) and ZSF1-Obese rats (for BW, LVEF%, E/A ratio, E/E' ratio and LW/TL ratio n=5 rats per group; for HW/TL ratio n=5 rats per WKY group and n=4 rats per ZSF1-Obese group). **m**, Electrophoretic analysis of spliced (s) and unspliced (u) Xbp1 transcript in LV samples from WKY and ZSF1-Obese rats. Tunicamycin-treated neonatal rat ventricular myocytes (TUN) were used as positive control (n=3 rats per group). **n**, LV mRNA levels of Xbp1s from WKY and ZSF1-Obese rats (n=5 rats per group). **o**, Immunoblot images of pIRE1α, IRE1α and GAPDH proteins from LV samples of WKY and ZF1-Obese rats (n=5 rats per group). **p**, Densitometric analysis ratio between pIRE1α and IRE1α protein bands (n=5 rats per group). Results are presented as mean±S.E.M. **a-e** One-way ANOVA followed by Sidak's multiple comparisons test. **g-l, n, p** Two-tailed unpaired Student's *t*-test. Numbers above square brackets show significant *P* values. For gel source data, see Supplementary Fig. 1.

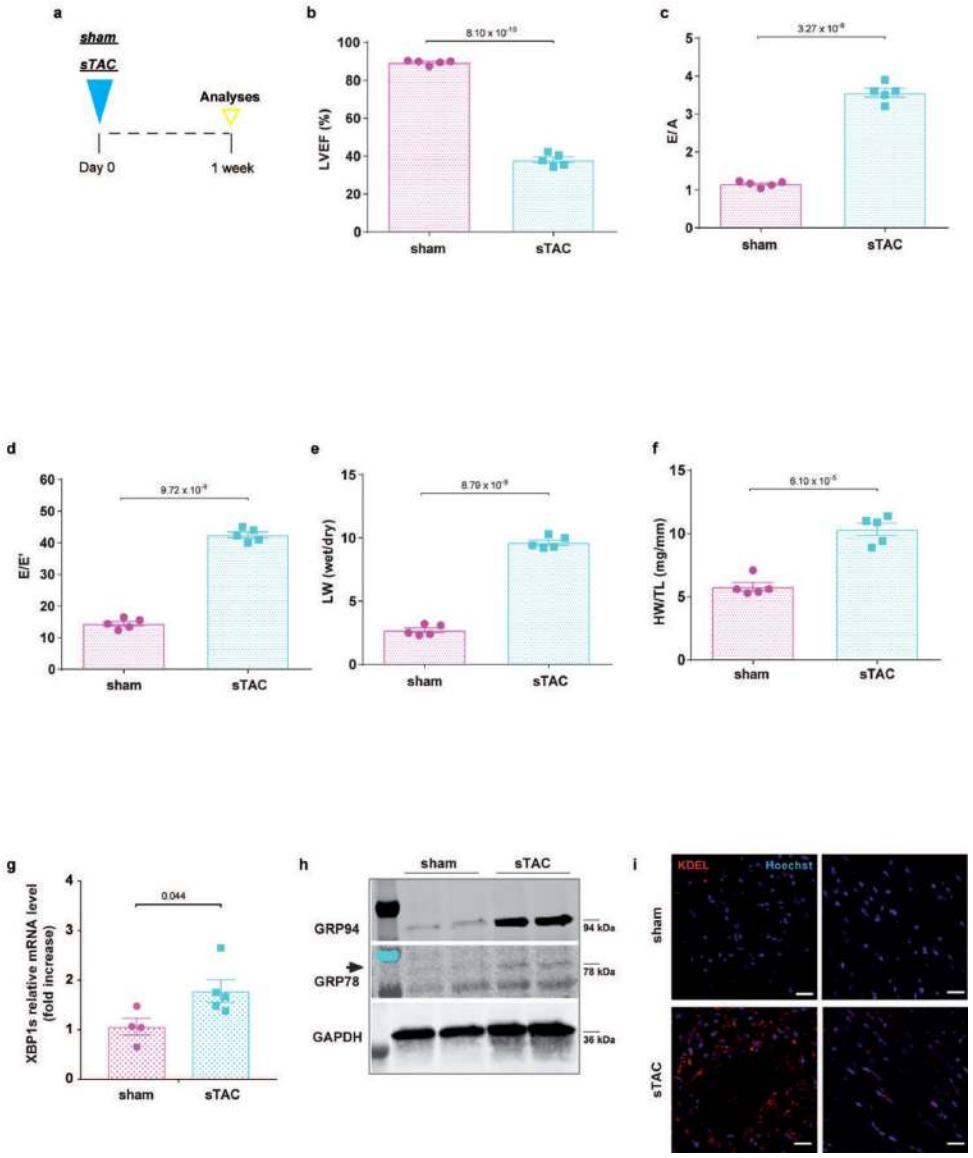

Extended Data Figure 5. Functional characterization and unfolded protein response activation in mice after one week of severe transverse aortic constriction.

a, Experimental design. C57BL/6N male mice were exposed to sham (control) or severe transverse aortic constriction (sTAC) surgery (filled triangle) and evaluated after one week (empty triangle). **b**, Percent left ventricular ejection fraction (LVEF%), **c**, Ratio between mitral E wave and A wave (E/A), **d**, Ratio between mitral E wave and E' wave (E/E'), **e**, Ratio between wet and dry lung weight (LW) and **f**, Ratio between heart weight and tibia length (HW/TL) of sham control and sTAC mice (n=5 mice per group). **g**, LV Xbp1s mRNA level from sham and sTAC mice (n=4 mice in sham group; n=5 mice in sTAC group). **h**, Immunoblot images of GRP94, GRP78 and GAPDH proteins in LV samples of sham and sTAC mice. Images are representative of three independently performed experiments with similar results. Arrow indicates the regulated band. **i**, KDEL (Lys-Asp-Glu-Leu) sequence immunofluorescence staining in LV sections of sham and sTAC mice. Hoechst stains nuclei. Scale bars: 50 μm. Images are representative of three independently performed experiments

with similar results. Results are presented as mean±S.E.M. **b-g** Two-tailed unpaired Student's *t*-test. Numbers above square brackets show significant *P* values. For gel source data, see Supplementary Fig. 1.

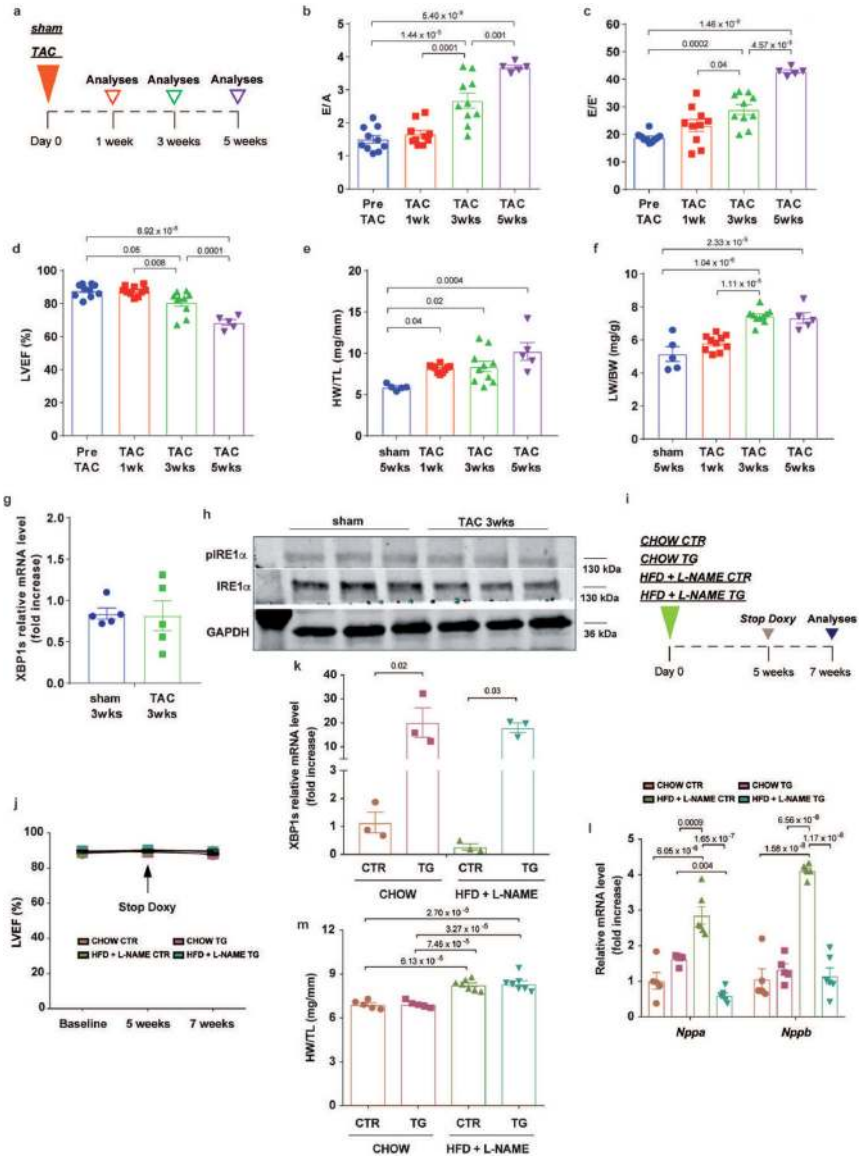

Extended Data Figure 6. Functional characterization and IRE1α-Xbp1s axis in mice after transverse aortic constriction and phenotype of cardiomyocyte-restricted Xbp1s transgenic mice.

a, Experimental design. C57BL/6N mice were exposed to sham (control) or transverse aortic constriction (TAC) surgery (filled triangle) and followed up to five weeks (empty triangles). **b**, Ratio between mitral E wave and A wave (E/A), **c**, Ratio between mitral E wave and E' wave (E/E'), **d**, Percent left ventricular ejection fraction (LVEF%), **e**, Ratio between heart weight and tibia length (HW/TL), and **f**, Ratio between lung weight and body weight (LW/BW) of different experimental groups of mice (for E/A ratio, E/E' ratio and LVEF% n=10 mice per Pre-TAC, TAC 1wk and TAC 3wks groups; n=5 mice per TAC 5wks group; for HW/TL ratio and LW/BW ratio n=10 mice per TAC 1wk and TAC 3wks groups; n=5 mice per sham and TAC 5wks groups). **g**, LV Xbp1s mRNA levels from sham and TAC 3wks (n=5 mice per group). **h**, Immunoblot images of pIRE1α, IRE1α and GAPDH proteins from LV samples of sham and TAC 3wks mice (n=3 mice per group). **i**, Experimental design. Control (CTR) and Xbp1s transgenic mice (TG) were exposed to

CHOW or HFD+L-NAME diet (green filled triangle). After five weeks, echocardiographic assessment was performed and doxycycline (Doxy) was removed from the drinking water to induce transgene expression (gray filled triangle). Two weeks after transgene induction (blue filled triangle), mice were subjected to functional analysis and tissue harvesting. **j**, LVEF% of different experimental cohorts over time (n=5 mice per CHOW CTR and CHOW TG groups; n=7 mice per HFD+L-NAME CTR and HFD+L-NAME TG groups. Each mouse was analyzed at all three time points). **k**, LV Xbp1s mRNA level in CTR and Xbp1s TG mice fed with CHOW or HFD+L-NAME diet for seven weeks (n=3 mice per group). **l**, LV mRNA levels of *nppa* and *nppb* genes and **m**, HW/TL at the end of the study (n=5 mice per CHOW CTR and CHOW TG groups; n=7 mice per HFD+L-NAME CTR and HFD+L-NAME TG groups). Results are presented as mean±S.E.M. **b-f**, One-way ANOVA followed by Sidak's multiple comparisons test. **g** Two-tailed unpaired Student's *t*-test. **j-m** Two-way ANOVA followed by Sidak's multiple comparisons test. Numbers above square brackets show significant *P* values. For gel source data, see Supplementary Fig. 1.

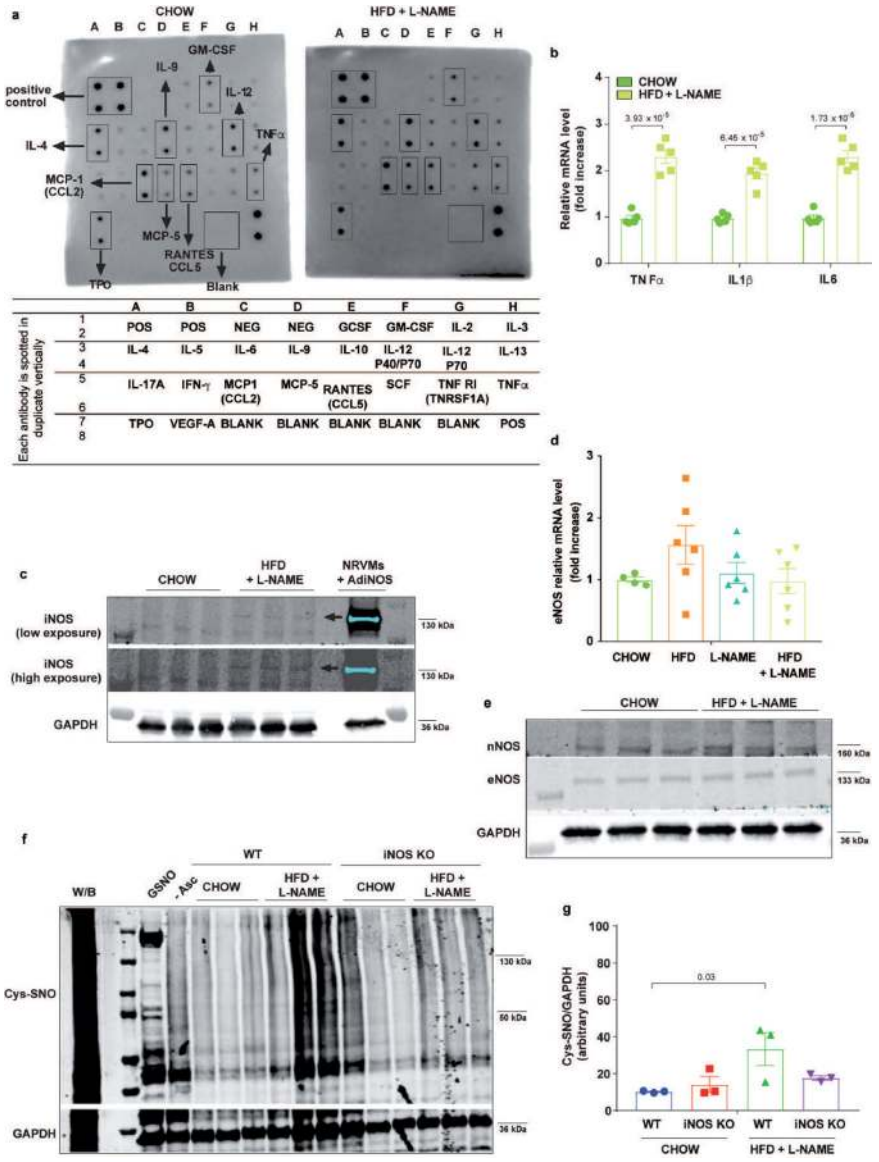

Extended Data Figure 7. Myocardial nitrosative stress and inflammatory markers in mice after five weeks of different dietary regimens.

a, *Top*: Cytokines/chemokines antibody array in plasma samples from CHOW and HFD+L-NAME mice with visual estimation of differently abundant cytokines. Each Images are representative of two independently performed experiments with similar results. *Bottom*: List of cytokines and chemokines represented by the antibody array membrane. **b**, Left ventricular (LV) TNFα, IL1β and IL6 mRNA levels of CHOW and HFD+L-NAME mice (n=5 mice per group). **c**, iNOS and GAPDH in LV samples of CHOW and HFD+L-NAME mice. Neonatal rat ventricular myocytes infected with mouse iNOS adenovirus (AdiNOS; 100 multiplicity of infection) were used as positive controls for iNOS bands. Arrow indicates the regulated band (n=3 mice per group). **d**, LV mRNA levels of eNOS of different experimental groups of mice (n=4 mice per CHOW group; n=6 mice per HFD, L-NAME and HFD+L-NAME groups). **e**, Immunoblot images of nNOS, eNOS and GAPDH proteins of different experimental groups of mice (n=3 mice per group). **f**, Immunoblot images of

nitrosylated cysteines (Cys-SNO) and GAPDH proteins in LV samples of wild type (WT) and iNOS knock out (iNOS KO) mice after five weeks of CHOW and HFD+L-NAME diet (W/B: without blocking. - Asc: without ascorbate. GSNO: S-Nitrosoglutathione) (n=3 mice per group). **g**, Densitometric analysis ratio between Cys-SNO/GAPDH proteins (n=3 mice per group). Results are presented as mean±S.E.M. **b**, Two-tailed unpaired Student's *t*-test. **d** One-way ANOVA followed by Sidak's multiple comparisons test. **g**, Two-way ANOVA followed by Sidak's multiple comparisons test. Numbers above square brackets show significant *P* values. For gel source data, see Supplementary Fig. 1.

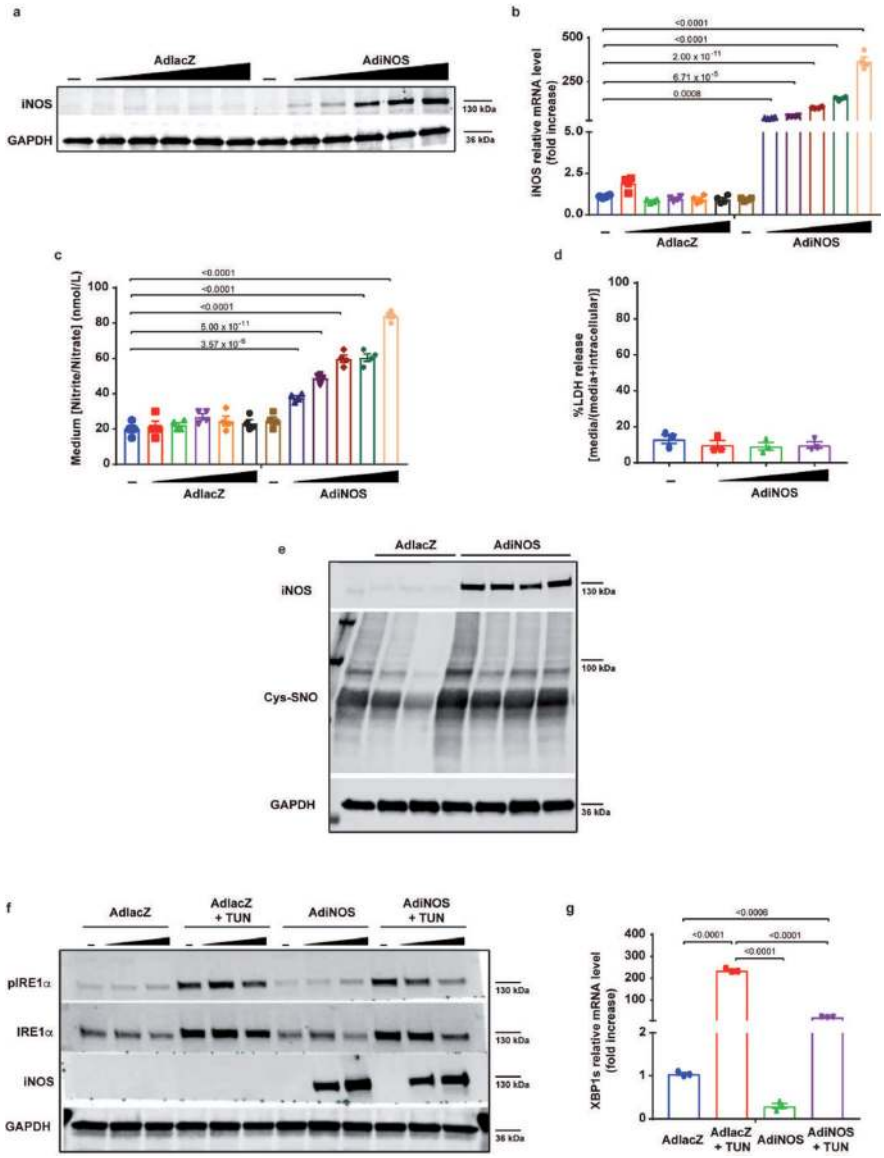

Extended Data Figure 8. iNOS overexpression in cardiomyocytes reduces IRE1α activation and Xbp1s levels without affecting cardiomyocyte viability.

a, Immunoblot images of iNOS and GAPDH proteins of neonatal rat ventricular myocytes infected with increasing multiplicity of infection (MOI) of α-galactosidase adenovirus (AdLacZ) or iNOS adenovirus (AdiNOS) for 24 hours. Images are representative of three independently performed experiments with similar results. **b**, iNOS mRNA levels in neonatal rat ventricular myocytes transduced with increasing MOI of AdlacZ or AdiNOS for 24 hours (n=4 biologically independent experiments). **c**, Medium nitrite/nitrate concentration of neonatal rat ventricular myocytes transduced with increasing MOI of AdlacZ or AdiNOS for 24 hours (n=4 biologically independent experiments). **d**, Lactate dehydrogenase (LDH) release in neonatal rat ventricular myocytes transduced with increasing MOI of AdlacZ or AdiNOS for 24 hours (n=3 biologically independent experiments). **e**, Immunoblot images of Cys-SNO, iNOS and GAPDH proteins in NRVMs transduced with AdlacZ or AdiNOS for 24 hours (100 MOI). Images are representative of

three independently performed experiments with similar results. **f**, Immunoblot images of pIRE1α, IRE1α, iNOS and GAPDH proteins in neonatal rat ventricular myocytes transduced with increasing MOI of AdlacZ or AdiNOS in the presence or absence of tunicamycin (TUN) for 24 hours. Images are representative of three independently performed experiments with similar results. **g**, Xbp1s mRNA level of neonatal rat ventricular myocytes transduced with 100 MOI of AdlacZ or AdiNOS in the presence or absence of TUN for 24 hours (n=3 biologically independent experiments). Results are presented as mean±S.E.M. **b-d, g** One-way ANOVA followed by Sidak's multiple comparisons test. Numbers above square brackets show significant *P* values. For gel source data, see Supplementary Fig. 1.

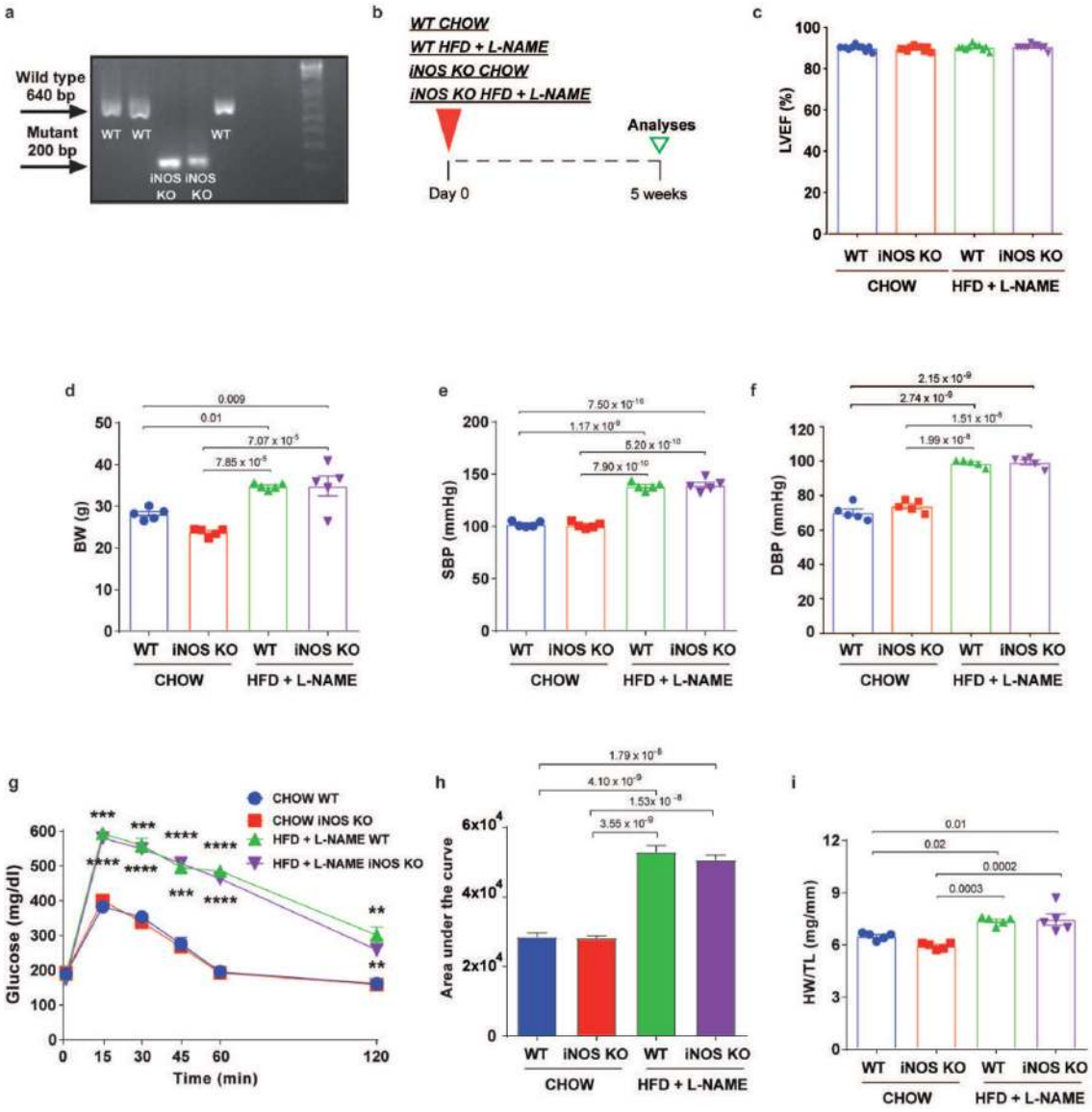

Extended Data Figure 9. Phenotype of iNOS knockout mice after five weeks of different dietary regimens.

a, DNA genotyping of wild type (WT) and iNOS knock out (iNOS KO) mice. This signature was used for genotyping. **b**, Experimental design. WT and iNOS KO mice were exposed to CHOW or HFD+L-NAME diet for five weeks (filled triangle). Subsequently, mice were subjected to functional analysis and tissue harvesting (empty triangle). **c**, Percent left ventricular ejection fraction (LVEF%), **d**, Body weight (BW), **e**, Systolic blood pressure (SBP), **f**, Diastolic blood pressure (DBP) and **g**, Intraperitoneal glucose tolerance test (ipGTT) of different experimental groups of mice (for LVEF% n=10 mice per group; for BW, SBP, DBP and ipGTT n=5 mice per group). **h**, Bar graphs depicting the area under the curve of the ipGTT experiment (n=5 mice per group). **i**, Ratio between heart weight and tibia length (HW/TL) of different experimental groups of mice (n=5 mice per group). Results are presented as mean±S.E.M. **c-i** Two-way ANOVA followed by Sidak's multiple comparisons test. **c-f, h, i** Numbers above square brackets show significant *P* values. **g**, 15'

***P=0.0002 CHOW WT vs. HFD+L-NAME WT, ****P<0.0001 CHOW WT vs. HFD+L-NAME iNOS KO; 30' ***P=0.0002 CHOW WT vs. HFD+L-NAME WT, ****P<0.0001 CHOW WT vs. HFD+L-NAME iNOS KO; 45' ****P<0.0001 CHOW WT vs. HFD+L-NAME WT, ***P=0.0002 CHOW WT vs. HFD+L-NAME iNOS KO; 60' ****P<0.0001 CHOW WT vs. HFD+L-NAME WT, ****P<0.0001 CHOW WT vs. HFD+L-NAME iNOS KO; 120' **P=0.010 CHOW WT vs. HFD+L-NAME WT, **P=0.007 CHOW WT vs. HFD +L-NAME iNOS KO. For gel source data, see Supplementary Fig. 1.

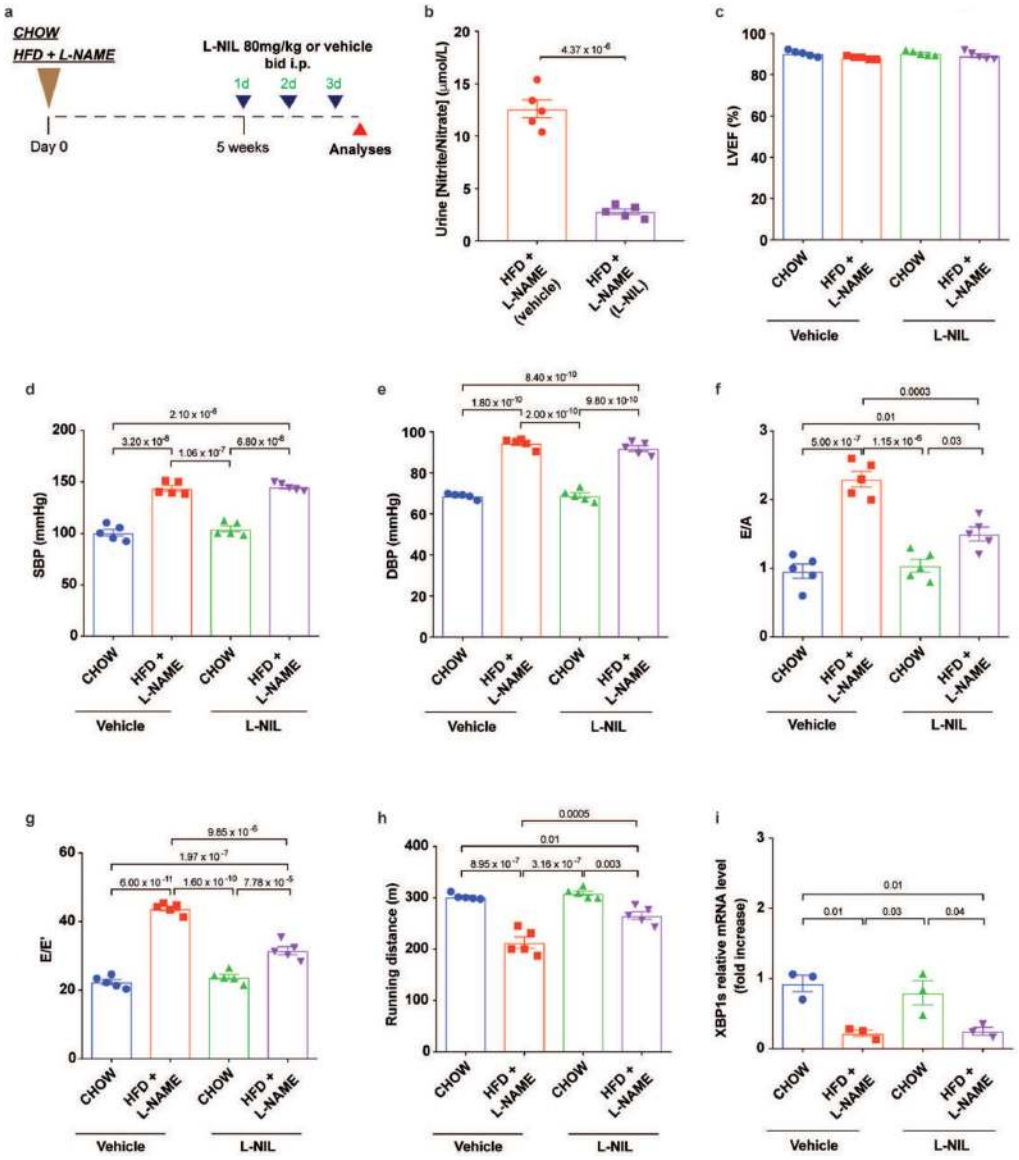

Extended Data Figure 10. Functional characterization and Xbp1s myocardial levels of mice treated with iNOS inhibitor.

a, Experimental design. C57BL/6N mice were exposed to CHOW or HFD+L-NAME diet (brown filled triangle) for five weeks and subsequently injected intraperitoneally (i.p.) with L-N6-(1-iminoethyl)lysine (L-NIL) at the dose of 80 mg/kg body weight or vehicle twice a day for three days (blue filled triangles). After that point, mice were subjected to functional analysis and tissue harvesting (red filled triangle). **b**, Urinary nitrite/nitrate concentration in HFD+L-NAME mice treated with vehicle or L-NIL (n=5 mice per group). **c**, Systolic blood pressure (SBP), **d**, Diastolic blood pressure (DBP), **e**, Percent left ventricular ejection fraction (LVEF%), **f**, Ratio between mitral E wave and A wave (E/A), **g**, Ratio between mitral E wave and E' wave (E/E'), **h**, Running distance during exercise exhaustion test and **i**, LV mRNA levels of Xbp1s of different experimental groups of mice (for nitrite/nitrate level, SBP, DBP, LVEF%, E/A, E/E' and running distance n=5 mice group; for Xbp1s level n=3 per group). Results are presented as mean±S.E.M. **b** Two-tailed unpaired Student's *t*-test. **c-i**

Two-way ANOVA followed by Sidak's multiple comparisons test. Numbers above square brackets show significant *P* values.

Extended Data Table 1.

Echocardiographic and invasive hemodynamic parameters in the different experimental groups of mice.

	CHOW	HFD	L-NAME	HFD + L-NAME
Echocardiography				
5-week treatment (n=10/group)				
Conscious				
HR (bpm)	688±15	696±19	677±19	685±17
LVID,d (mm)	2.7±0.2	2.8±0.1	2.9±0.3	2.9±0.2
LVID,s (mm)	1.0±0.1	1.1±0.3	1.1±0.2	1.2±0.1
IVS,d (mm)	1.1±0.1	1.1±0.1	1.3±0.1	1.3±0.2
LVPW,d (mm)	0.9±0.1	1.0±0.2	1.1±0.2	1.1±0.1
LVFS (%)	59.2±2.2	60.7±2.3	62.0±1.3	58.6±1.6
LV mass (mg) LVEF (%)	88.8±5.7	101.0±8.3	131.3±9.4†	131.3±7.5†
Unconscious	85.9±0.8	87.6±1.0	87.1±0.6	86.3±1.0
HR (bpm)	423±16	445±20	432±12	445±19
Peak mitral E velocity (mm/sec)	443.6±13.3	503.4±10.6†	633.0±12.5§	847.2±8.6§,*
Peak mitral A velocity (mm/sec)	433.2±8.2	450.8±7.4	361.5±9.9†	442.6±8.3$^{\#}$
Mitral E/A	1.0±0.04	1.1±0.03	1.8±0.04§	1.9±0.06§,*
IVRT (mm/sec)	21.3±2.1	20.4±1.4	15.6±1.3	14.9±1.9*
Mitral DT (msec)	22.4±1.1	21.4±2.1	16.5±1.2*	15.7±1.3†
Peak mitral E' velocity (mm/sec)	26.5±0.5	27.6±0.8	21.8±0.5§	20.1±0.9§
Mitral E/E'	16.6±1.0	18.2±0.9	28.8±1.1§	42.5±2.3§,*
15-week treatment (n=15/group)				
Conscious				
HR (bpm)	667±14	687±15	698±19	677±13
LVID,d (mm)	2.8±0.1	2.9±0.3	3.0±0.4	3.1±0.2
LVID,s (mm)	1.1±0.1	1.2±0.2	1.2±0.1	1.3±0.1
IVS,d (mm)	1.0±0.2	1.1±0.2	1.4±0.2	1.4±0.3
LVPW,d (mm)	0.9±0.1	1.0±0.2	1.1±0.1	1.1±0.2
LVFS (%)	60.7±1.3	58.6±1.5	60.0±1.3	58.1±1.4
LV mass (mg)	86.4±6.5	106.1±7.8	147.0±8.4§	153.8±10.3§
LVEF (%)	89.3±0.4	89.7±0.4	89.3±0.6	88.7±0.7
Unconscious	433±12.4	442±13.4	421±11.2	436±12.3
HR (bpm)	603.0±8.22	544.5±9.3§	755.8±5.1§	998.2±2.5§,*
Peak mitral E velocity (mm/sec)	443.3±7.9	560.2±8.0§	431.9±4.6	386.5±4.2§
Peak mitral A velocity (mm/sec)	1.4±0.02	1.0±0.02§	1.8±0.02§	2.6±0.03§,*
Mitral E/A	20.3±1.8	24.5±2.1	16.5±1.3	13.2±1.4*
IVRT (mm/sec)	23.2±1.3	26.5±1.1	16.9±1.5†	14.4±1.0§
Mitral DT (msec)	25.8±0.4	22.2±0.4§	19.7±0.2§	20.7±0.4§

	CHOW	HFD	L-NAME	HFD + L-NAME
Peak mitral E' velocity (mm/sec) Mitral E/E'	23.5±0.5	24.7±0.6	38.5±0.5§	48.4±0.8§,*
LVEF (%) time course				
- *24-week treatment (*n=5/group)	90.7±0.2	N/A	N/A	88.62±0.4
- *50-week treatment (*n=5/group)	90.1±0.1	N/A	N/A	90.1±0.4
Invasive hemodynamic analysis				
15-week treatment (n=3/group)				
ESP, mm Hg	93.4±1.4	98.8±1.2	114.3±5.6†	130.9±2.7$^{\ddagger,/\!/}$
EDP, mm Hg	1.4±0.06	1.3±0.06	3.6±0.1†	4.3±0.1$^{\ddagger,\#}$
dPmax, mm Hg/s	10234±345	9674±456	10324±435	9893±453
dPmin, mm Hg/s	–9834±534	–10456±521	–9987±432	–10156±367
Ea, mm Hg/μL	2.5±0.1	2.6±0.2	3.0±0.1*	3.6±0.1$^{\ddagger,/\!/}$
Ees, mm Hg/μL	3.8±0.4	3.7±0.3	5.1±0.2*	5.0±0.1*
EDPVR, mm Hg/μL	0.028±0.003	0.027±0.002	0.068±0.005†	0.093±0.004$^{\S,\#}$

Results are presented as mean±SEM. One-way ANOVA plus Sidak's multiple comparisons test was used to detect significance.

*p<0.05 vs. CHOW

†p<0.01 vs. CHOW

‡p<0.0001 vs. CHOW

§p<0.00001 vs. CHOW

$^{/\!/}$p<0.05 vs. L-NAME

¶p<0.01 vs. L-NAME

$^{\#}$p<0.001 vs. L-NAME

*p<0.0001 vs. L-NAME.

Abbreviations used: **HR**, heart rate; **LVID,d**, left ventricular internal diastolic diameter; **LVID,s**, left ventricular internal systolic diameter; **IVS,d**, end-diastolic interventricular septal wall thickness; **LVPW,d**, left ventricular end-diastolic posterior wall; **LVFS**, left ventricular fractional shortening; **LV mass**, left ventricular mass; **LVEF**, left ventricular ejection fraction; **E**, peak Doppler blood inflow velocity across mitral valve during early diastole; **A**, peak Doppler blood inflow velocity across mitral valve during late diastole; **IVRT**, isovolumic relaxation time; **DT**, early filling deceleration time; **E'**, peak tissue Doppler of myocardial relaxation velocity at mitral valve annulus during early diastole; **ESP**, end-systolic pressure; **EDP**, end-diastolic pressure; **dP max**, maximal rate of pressure rise; **dPmin**, maximal rate of pressure decline; **Ea**, effective arterial elastance; **Ees**, slope of end-systolic pressure-volume relation; **EDPVR**, end-diastolic pressure-volume relation; **N/A**, data not available.

Extended Data Table 2.

Clinical characteristics of CTR, HFpEF and HFrEF subjects.

	CTR (n=12)	HFpEF (n=13)	HFrEF (n=15)	p values
Demographics				
Age, (years), mean±SD	55.3±13.0	66.0±10.7	50.4±16.1	0.015
Female, n (%)	4 (33.3)	11 (91.6)	3 (20.0)	0.002
Ethnicity, n (%)				
- White	9 (75.0)	4 (30.7)	11 (75.0)	0.032
- Black	2 (16.6)	8 (61.5)	4 (26.6)	0.044
- Hispanic	1 (8.3)	1 (7.7)	0 (0)	0.530

	CTR (n=12)	HFpEF (n=13)	HFrEF (n=15)	p values
Height, (m), mean±SD	1.7±0.1	1.6±0.1	1.7±0.1	0.019
Weight, (kg), mean±SD	82.8±28.5	103.3±20.1	82.1±23.7	0.049
BMI, (kg/m2), mean±SD	29.4±9.0	39.0±7.1	26.6±5.3	0.0002
EF, (%), mean±SD	62.0±2.4	64.6±6.3	17.1±6.1	<0.0001
Medical history				
Smoking, n (%)	N/A	4 (30.7)	N/A	N/A
Hypertension, n (%)	5 (41.6)	13 (100)	15 (100)	0.00005
Diabetes, n (%)	2 (16.6)	10 (76.9)	2 (13.3)	0.001
Coronary artery disease, n (%)	1 (8.3)	4 (30.7)	3 (20)	0.375
Chronic kidney disease, n (%)	2 (16.6)	10 (76.9)	3 (20)	0.002
Hyperlipidemia, n (%)	N/A	9 (69.2)	N/A	N/A
Atrial fibrillation, n (%)	1 (8.3)	3 (23.0)	1 (6.6)	0.078
Medications				
Diuretics, n (%)	0 (0)	13 (100)	15 (100)	<0.0001
ACEIs, n (%)	4 (33.3)	0 (0)	8 (53.3)	0.009
ARBs, n (%)	0 (0)	7 (53.8)	6 (40)	0.012
Beta blockers, n (%)	3 (25)	9 (69.2)	14 (93.3)	0.001
Nitrate, n (%)	0 (0)	0 (0)	2 (13.3)	0.173
Insulin, n (%)	0 (0)	6 (46.1)	1 (6.6)	0.004

Results are presented as mean±SD for continuous variables and number (n) and percentage (%) for categorical variables. For continuous variables one-way ANOVA was used to detect significance. For categorical variables two-sided chi-square test was used to detect significance. **Abbreviations used: m**, meters; **kg**, kilograms; **BMI**, body mass index; **EF**, ejection fraction; **ACEIs**, angiotensin-converting enzyme inhibitors; **ARBs**, angiotensin receptor blockers; **N/A**, data not available.

Supplementary Material

Refer to Web version on PubMed Central for supplementary material.

Acknowledgements.

This work was supported by grants from NIH: HL-120732 (J.A.H.), HL-100401 (J.A.H.), HL-097768 (J.A.H.), F32HL136151 (K.M.F.), F32HL142244 (D.T.), HL-135827 (D.A.K.), HL-119012 (D.A.K.), HL-07227 (V.H.), American Heart Association (AHA): 16POST30680016 (F.A.), 16PRE29660003 (S.Y.K.), 14SFRN20510023 (J.A.H.), 14SFRN20670003 (J.A.H.), and 16SFRN28620000 (K.S., D.A.K.), AHA and the Theodore and Beulah Beasley Foundation 18POST34060230 (G.G.S.), University Federico II of Naples and Compagnia di San Paolo STAR program (G.G.S.), Fondation Leducq TransAtlantic Network of Excellence11CVD04 (J.A.H.), Cancer Prevention and Research Institute of Texas RP110486P3 (J.A.H.) and by Fondo Nacional de Desarrollo Científico y Tecnológico, FONDAP 15130011 (S.L.). We thank Gökhan S. Hotamisligil and Ling Yang for providing IRE1α WT and IRE1α M1+M2 expressing adenoviruses.

References

1. Dunlay SM, Roger VL & Redfield MM Epidemiology of heart failure with preserved ejection fraction. Nat Rev Cardiol, doi:10.1038/nrcardio.2017.65 (2017).

2. Shah SJ et al. Phenotype-Specific Treatment of Heart Failure With Preserved Ejection Fraction: A Multiorgan Roadmap. Circulation 134, 73–90, doi:10.1161/CIRCULATIONAHA.116.021884 (2016). [PubMed: 27358439]

3. Chirinos JA & Zamani P The Nitrate-Nitrite-NO Pathway and Its Implications for Heart Failure and Preserved Ejection Fraction. Curr Heart Fail Rep 13, 47–59, doi:10.1007/s11897-016-0277-9 (2016). [PubMed: 26792295]

4. Butler J, Braunwald E & Gheorghiade M Recognizing worsening chronic heart failure as an entity and an end point in clinical trials. JAMA 312, 789–790, doi:10.1001/jama.2014.6643 (2014). [PubMed: 25157719]

5. Roh J, Houstis N & Rosenzweig A Why Don't We Have Proven Treatments for HFpEF? Circ Res 120, 1243–1245, doi:10.1161/CIRCRESAHA.116.310119 (2017). [PubMed: 28408453]

6. Primessnig U et al. Novel pathomechanisms of cardiomyocyte dysfunction in a model of heart failure with preserved ejection fraction. Eur J Heart Fail 18, 987–997, doi:10.1002/ejhf.524 (2016). [PubMed: 27135883]

7. Methawasin M et al. Experimentally Increasing the Compliance of Titin Through RNA Binding Motif-20 (RBM20) Inhibition Improves Diastolic Function In a Mouse Model of Heart Failure With Preserved Ejection Fraction. Circulation 134, 1085–1099, doi:10.1161/CIRCULATIONAHA.116.023003 (2016). [PubMed: 27630136]

8. Gonzalez-Lopez E et al. Wild-type transthyretin amyloidosis as a cause of heart failure with preserved ejection fraction. Eur Heart J 36, 2585–2594, doi:10.1093/eurheartj/ehv338 (2015). [PubMed: 26224076]

9. Wang ZV & Hill JA Protein quality control and metabolism: bidirectional control in the heart. Cell Metab 21, 215–226, doi:10.1016/j.cmet.2015.01.016 (2015). [PubMed: 25651176]

10. Wang ZV et al. Spliced X-box binding protein 1 couples the unfolded protein response to hexosamine biosynthetic pathway. Cell 156, 1179–1192, doi:10.1016/j.cell.2014.01.014 (2014). [PubMed: 24630721]

11. Rothermel BA et al. Differential activation of stress-response signaling in load-induced cardiac hypertrophy and failure. Physiol Genomics 23, 18–27, doi:10.1152/physiolgenomics.00061.2005 (2005). [PubMed: 16033866]

12. Paulus WJ & Tschope C A novel paradigm for heart failure with preserved ejection fraction: comorbidities drive myocardial dysfunction and remodeling through coronary microvascular endothelial inflammation. J Am Coll Cardiol 62, 263–271, doi:10.1016/j.jacc.2013.02.092 (2013). [PubMed: 23684677]

13. Furfine ES, Harmon MF, Paith JE & Garvey EP Selective inhibition of constitutive nitric oxide synthase by L-NG-nitroarginine. Biochemistry 32, 8512–8517 (1993). [PubMed: 7689333]

14. Kopincova J, Puzserova A & Bernatova I L-NAME in the cardiovascular system - nitric oxide synthase activator? Pharmacol Rep 64, 511–520 (2012). [PubMed: 22814004]

15. Yang L et al. METABOLISM. S-Nitrosylation links obesity-associated inflammation to endoplasmic reticulum dysfunction. Science 349, 500–506, doi:10.1126/science.aaa0079 (2015). [PubMed: 26228140]

16. Gould N, Doulias PT, Tenopoulou M, Raju K & Ischiropoulos H Regulation of protein function and signaling by reversible cysteine S-nitrosylation. J Biol Chem 288, 26473–26479, doi:10.1074/jbc.R113.460261 (2013). [PubMed: 23861393]

17. Moore WM et al. L-N6-(1-iminoethyl)lysine: a selective inhibitor of inducible nitric oxide synthase. J Med Chem 37, 3886–3888 (1994). [PubMed: 7525961]

18. Borlaug BA, Koepp KE & Melenovsky V Sodium Nitrite Improves Exercise Hemodynamics and Ventricular Performance in Heart Failure With Preserved Ejection Fraction. J Am Coll Cardiol 66, 1672–1682, doi:10.1016/j.jacc.2015.07.067 (2015). [PubMed: 26449137]

19. Sharma K & Kass DA Heart failure with preserved ejection fraction: mechanisms, clinical features, and therapies. Circ Res 115, 79–96, doi:10.1161/CIRCRESAHA.115.302922 (2014). [PubMed: 24951759]

20. Redfield MM et al. Isosorbide Mononitrate in Heart Failure with Preserved Ejection Fraction. N Engl J Med 373, 2314–2324, doi:10.1056/NEJMoa1510774 (2015). [PubMed: 26549714]

21. Zamani P et al. Isosorbide Dinitrate, With or Without Hydralazine, Does Not Reduce Wave Reflections, Left Ventricular Hypertrophy, or Myocardial Fibrosis in Patients With Heart Failure With Preserved Ejection Fraction. J Am Heart Assoc 6, doi:10.1161/JAHA.116.004262 (2017).

22. Oeser C Heart failure: Nitrates reduce activity levels in HFpEF. Nat Rev Cardiol 13, 2, doi: 10.1038/nrcardio.2015.176 (2016).

23. Jia J et al. Target-selective protein S-nitrosylation by sequence motif recognition. Cell 159, 623–634, doi:10.1016/j.cell.2014.09.032 (2014). [PubMed: 25417112]

24. Zhu H et al. Cardiac autophagy is a maladaptive response to hemodynamic stress. J Clin Invest 117, 1782–1793, doi:10.1172/JCI27523 (2007). [PubMed: 17607355]

25. Kong Y et al. Suppression of class I and II histone deacetylases blunts pressure-overload cardiac hypertrophy. Circulation 113, 2579–2588, doi:10.1161/CIRCULATIONAHA.106.625467 (2006). [PubMed: 16735673]

26. Oh M et al. Calcineurin is necessary for the maintenance but not embryonic development of slow muscle fibers. Molecular and cellular biology 25, 6629–6638, doi:10.1128/MCB. 25.15.6629-6638.2005 (2005). [PubMed: 16024798]

27. Zhi G et al. Myosin light chain kinase and myosin phosphorylation effect frequency-dependent potentiation of skeletal muscle contraction. Proc Natl Acad Sci U S A 102, 17519–17524, doi: 10.1073/pnas.0506846102 (2005). [PubMed: 16299103]

28. Wang JM et al. IRE1alpha prevents hepatic steatosis by processing and promoting the degradation of select microRNAs. Sci Signal 11, doi:10.1126/scisignal.aao4617 (2018).

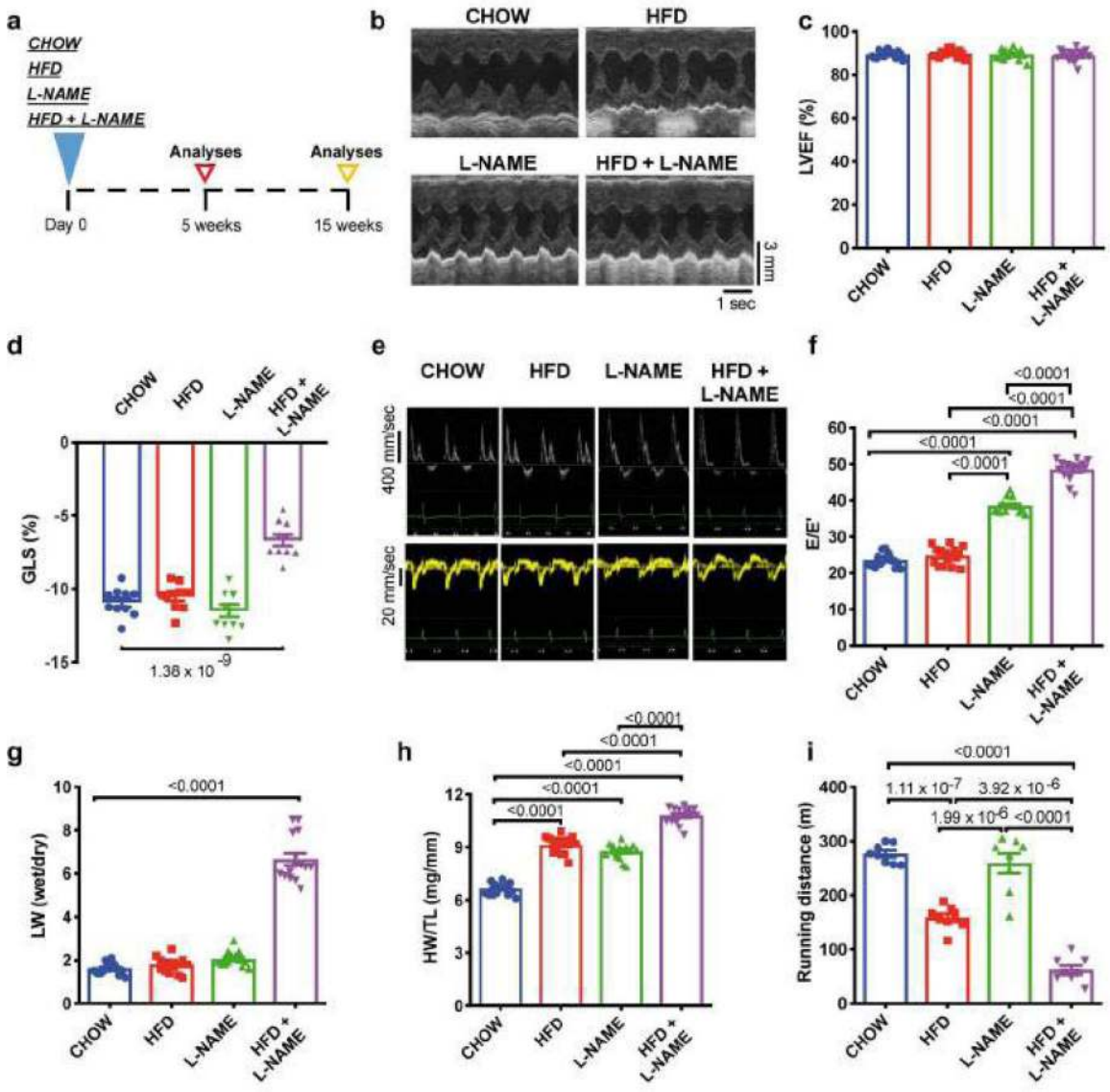

Figure 1. Fifteen weeks of HFD+L-NAME dietary regimen in mice recapitulates key alterations of clinical HFpEF.

a, Experimental design. C57BL/6N mice were maintained on different dietary regimens (filled triangle) and followed up to fifteen weeks (empty triangles). **b**, Representative left ventricular (LV) M-mode echocardiographic tracings. Images are representative of fifteen independent mice. **c**, Percent LV ejection fraction (LVEF%) (n=15 mice per group). **d**, LV global longitudinal strain (GLS) (n=10 mice per group). **e**, Representative pulsed-wave Doppler (top) and tissue Doppler (bottom) tracings. Images are representative of fifteen independent mice. **f**, Ratio between mitral E wave and E' wave (E/E') (n=15 mice per group). **g**, Ratio between wet and dry lung weight (LW) (n=15 mice per group). **h**, Ratio between heart weight and tibia length (HW/TL) (n=15 mice per group). **i**, Running distance during exercise exhaustion test (n=8 mice per group). Results are presented as mean±S.E.M. **c**, **d**, **f-i** One-way ANOVA followed by Sidak's multiple comparisons test. Numbers above square brackets show significant *P* values.

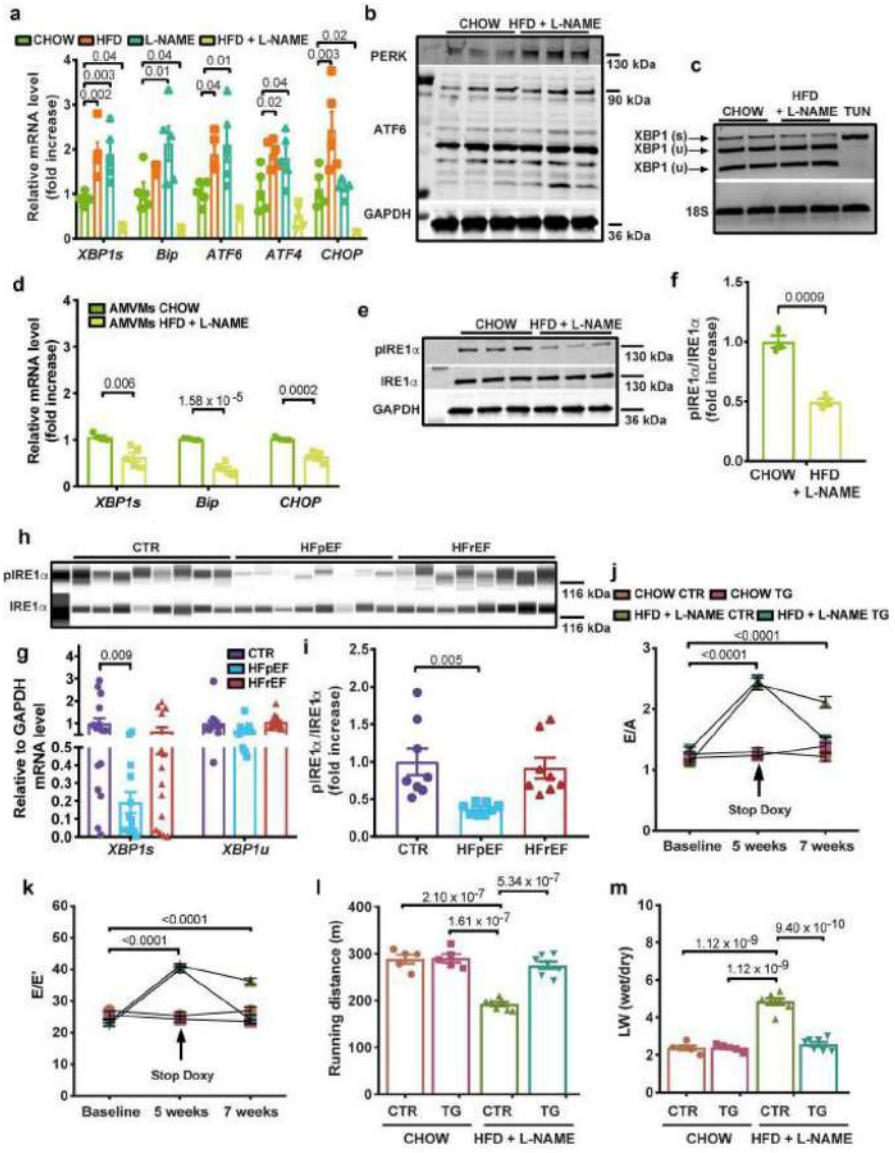

Figure 2. IRE1α-Xbp1s signaling pathway is inactive in experimental and human HFpEF and Xbp1s overexpression in cardiomyocytes ameliorates experimental HFpEF

a, Left ventricular (LV) mRNA levels of Xbp1s, Bip, ATF6, ATF4, CHOP in mice of different experimental groups (n=5 mice per group). **b**, Immunoblot images of PERK, ATF6 and GAPDH proteins in LV samples of CHOW and HFD+L-NAME mice (n=3 mice per group). **c**, Electrophoretic analysis of spliced (s) and unspliced (u) Xbp1 transcript in LV samples of CHOW and HFD+L-NAME mice. Tunicamycin-treated neonatal rat ventricular myocytes (TUN) were used as positive control. Images are representative of three independently performed experiments with similar results. **d**, Adult mouse ventricular myocytes (AMVMs) mRNA levels of Xbp1s, Bip, CHOP in CHOW and HFD+L-NAME mice (n=4 mice per CHOW group; n=5 mice per HFD+L-NAME group. AMVMs were isolated from individual mice). **e**, Immunoblot images of LV pIRE1α, IRE1α and GAPDH proteins of CHOW and HFD+L-NAME mice (n=3 mice per group). **f**, Densitometric analysis ratio between pIRE1α and IRE1α protein bands (n=3 mice per group). **g**, mRNA

levels of Xbp1s and Xbp1u in human myocardial biopsies from non-failing (CTR), HFpEF and HFrEF subjects (for CTR group n=15 subjects, for HFpEF group n=13 (Xbp1s) and n=14 (Xbp1u) subjects and for HFrEF group n=15). **h**, Immunoblot images of pIRE1α and IRE1α proteins in human myocardial biopsies from CTR, HFpEF and HFrEF subjects (n=8 subjects per group). **i**, Densitometric analysis ratio between pIRE1α and IRE1α protein bands (n=8 subjects per group). **j**, Ratio between mitral E wave and A wave (E/A) and **k**, Ratio between mitral E wave and E' wave (E/E') of control (CTR) and Xbp1s transgenic mice (TG) fed with CHOW or HFD+L-NAME diet over time (n=5 mice per CHOW CTR and CHOW TG groups; n=7 mice per HFD+L-NAME CTR and HFD+L-NAME TG groups. Each mouse was analyzed at all three time points). **l**, Running distance during exercise exhaustion test and **m**, Ratio between wet and dry lung weight (LW) at the end of the study (n=5 mice per CHOW CTR and CHOW TG groups; n=7 mice per HFD+L-NAME CTR and HFD+L-NAME TG groups). Results are presented as mean±S.E.M. **a, g, i** One-way ANOVA followed by Sidak's multiple comparisons test. **d**, **f**, Two-tailed unpaired Student's *t*-test. **j-m** Two-way ANOVA followed by Sidak's multiple comparisons test. Numbers above square brackets show significant *P* values. For gel source data, see Supplementary Fig. 1.

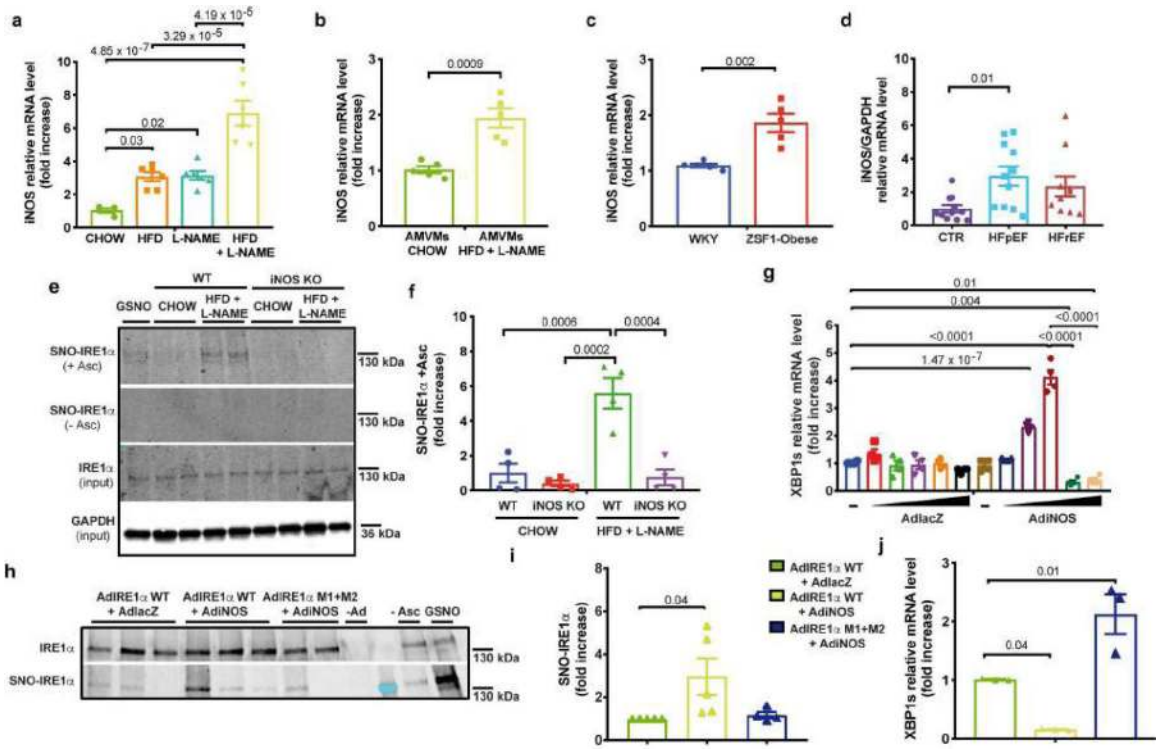

Figure 3. iNOS-dependent IRE1α nitrosylation in HFpEF and cardiomyocytes.

a, Left ventricular (LV) mRNA levels of iNOS of different experimental groups of mice (n=4 mice per CHOW group; n=6 mice per HFD, L-NAME and HFD+L-NAME groups **b**, Adult mouse ventricular myocytes (AMVMs) mRNA levels of iNOS CHOW and HFD+L-NAME mice (n=5 mice per group. AMVMs were isolated from individual mice). **c**, LV mRNA levels of iNOS from WKY and ZSF1-Obese rats (n=5 rats per group). **d**, mRNA levels of iNOS in human myocardial biopsies from non-failing (CTR), HFpEF and HFrEF subjects (n=11 subjects per CTR group, n=11 subjects per HFpEF group and n=10 subjects per HFrEF group). **e**, Immunoblot images of S-nitrosylated IRE1α (SNO-IRE1α), IRE1α and GAPDH proteins in LV samples of wild type (WT) and iNOS knock out (iNOS KO) mice after five weeks of CHOW or HFD+L-NAME diet. Images are representative of four independently performed experiments with similar results. (- Asc: without Ascorbate, + Asc: with Ascorbate GSNO: S-Nitrosoglutathione) **f**, Densitometric analysis SNO-IRE1α +Ascorbate protein bands in each group (n=4 mice per group). **g**, Xbp1s mRNA level of neonatal rat ventricular myocytes transduced with increasing multiplicity of infection of of α-galactosidase adenovirus (AdLacZ) or iNOS adenovirus (AdiNOS) for 24 hours (n=4 biologically independent experiments). **h**, Immunoblot images of SNO-IRE1α and IRE1α proteins in neonatal rat ventricular myocytes transduced with adenovirus for IRE1α wild type (AdIRE1α WT) or AdIRE1α mutated in two target nitrosylation sites (AdIRE1α M1+M2) and AdlacZ or AdiNOS for 24 hours (- Asc: No Ascorbate. GSNO: S-Nitrosoglutathione). Images are representative of three independently performed experiments with similar results. **i**, Densitometric analysis ratio between SNO-IRE1α and IRE1α protein band intensities (n=3 biologically independent experiments). **j**, Xbp1s mRNA level of neonatal rat ventricular myocytes transduced with AdIRE1α WT or AdIRE1α

M1+M2 and AdlacZ or AdiNOS for 24 hours (n=5 biologically independent experiments). Results are presented as mean±S.E.M. **a, d, g, i, j** One-way ANOVA followed by Sidak's multiple comparisons test. **b, c** Two-tailed unpaired Student's *t*-test. **f**, Two-way ANOVA followed by Sidak's multiple comparisons test. Numbers above square brackets show significant *P* values. For gel source data, see Supplementary Fig. 1.

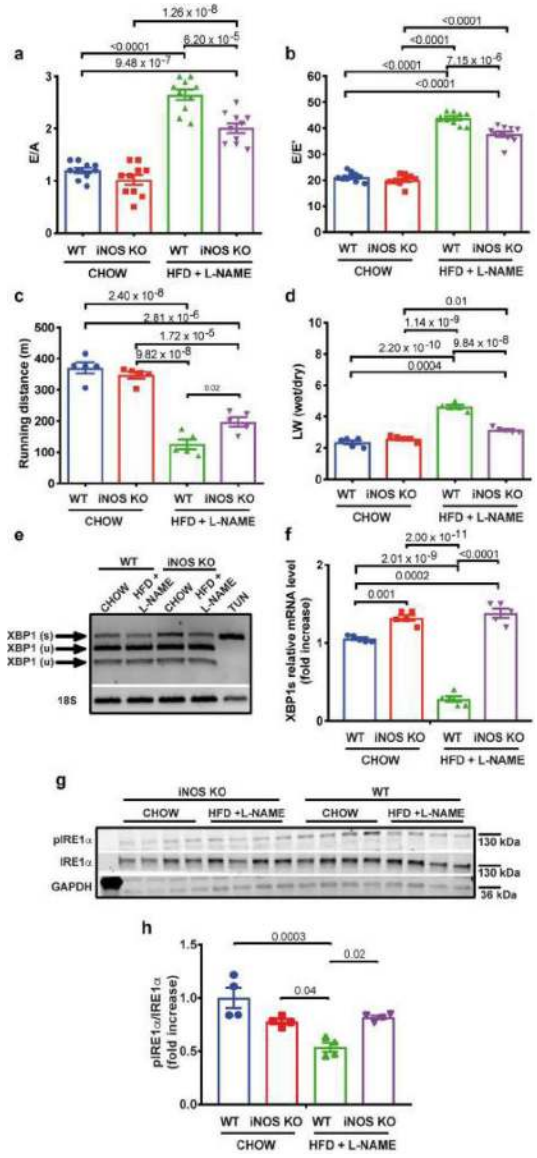

Figure 4. iNOS genetic inhibition ameliorate the HFpEF phenotype and restores IRE1α-Xbp1s signaling pathway in HFpEF.

a, Ratio between mitral E wave and A wave (E/A), **b**, Ratio between mitral E wave and E' wave (E/E'), **c**, Running distance during exercise exhaustion test, and **d**, Ratio between wet and dry lung weight (LW) of wild type (WT) and iNOS knock out (iNOS KO) mice after five weeks of CHOW or HFD+L-NAME diet (for E/A ratio, E/E' ratio n=10 mice per group; for running distance and LW wet/LW dry ratio n=5 mice per group). **e**, Electrophoretic analysis of spliced (s) and unspliced (u) Xbp1 transcript in left ventricular (LV) samples of WT and iNOS KO mice after five weeks of CHOW or HFD+L-NAME diet. Tunicamycin-treated neonatal rat ventricular myocytes (TUN) were used as positive control. Images are representative of three independently performed experiments with similar results. **f**, LV mRNA levels of Xbp1s (n=5 mice per group) and **g**, Immunoblot images of pIRE1α, IRE1α and GAPDH proteins in LV samples of WT and iNOS KO mice after five weeks of CHOW or HFD+L-NAME diet (n=4 mice per group). **h**, Densitometric analysis ratio between

pIRE1α and IRE1α protein bands (n=4 mice per group). Results are presented as mean ±S.E.M. **a-d, f, h** Two-way ANOVA followed by Sidak's multiple comparisons test. Numbers above square brackets show significant *P* values. For gel source data, see Supplementary Fig. 1.